A Novel 2:3 Condensation Complex of Salicylaldoxime and Di-*n*-butyltin(IV) Oxide

François Kayser,[†,‡] Monique Biesemans,[†,‡] Mohammed Bouâlam,[§,∥] Edward R. T. Tiekink,[⊥] Abdelaziz El Khloufi,[‡] Jacqueline Meunier-Piret,[△] Abdeslam Bouhdid,[‡] Klaus Jurkschat,[○] Marcel Gielen,[‡,§] and Rudolph Willem*[,†,‡]

High Resolution NMR Centre and Department of General and Organic Chemistry of the Faculty of Engineering, Free University of Brussels, VUB, Brussels, Belgium, Department of Organic Chemistry, Free University of Brussels, ULB, Brussels, Belgium, Department of Chemistry, The University of Adelaide, Adelaide, Australia, Laboratory of Physical Chemistry and Crystallography, Catholic University of Louvain, Louvain-la-Neuve, Belgium, and Department of Chemistry, Martin-Luther University, Halle/S., Germany

Received July 14, 1993[⊛]

The crystal structure of the reaction product of the 2:3 condensation of salicylaldoxime with di-*n*-butyltin(IV) oxide, [(Bu_2Sn)(Bu_2SnO)(Bu_2SnOH)(HONZO)(ONZO)], where HONZOH represents HON=CHC_6H_4OH (salicylaldoxime), was determined by single-crystal X-ray diffraction; it belongs to the monoclinic system, space group $P2_1/c$, with a = 20.995(3) Å, b = 17.394(4) Å, c = 12.254(2) Å, β = 94.43(2)°, and Z = 4. The compound contains two five-coordinate trigonal-bipyramidal tin atoms with the two butyl groups in equatorial positions; the third tin atom has a seven-coordinate pentagonal-bipyramidal geometry with the two butyl groups in apical positions. The bonds of the salicylaldoxime ligands to the metal atoms are inequivalent. Both ligands are bound to the seven-coordinate tin atom through the oxygen atom originating from the phenolic function and through the nitrogen atom of the aldoxime function. In the ligand that binds as HONZO, the phenolate oxygen atom further coordinates a five-coordinate tin atom. In the ligand that coordinates as ONZO, the NO oxygen is bonded to the other five-coordinate atom. The ^1H, ^{13}C, and ^{119}Sn NMR data are in agreement with such a structure existing as a major species M in solution. However, the NMR spectra also reveal the presence of three other minor species in solution, m_1, m_2, and m_3. These species could not be isolated as pure compounds, as crystallization from any solution of this compound led systematically to crystals of M. The ^1H and ^{119}Sn spectra, the $^nJ(^{119}Sn–^{119/117}Sn)$ coupling satellite patterns observed in ^{119}Sn spectra, and the two-dimensional proton detected $^1H–^{119}Sn$ heteronuclear multiple bond correlation (2D $^1H–^{119}Sn$ HMBC) maps allow us to propose a structure for each species.

Introduction

When diorganotin oxides $(R_2SnO)_n$ react with carboxylic acids R′COOH, several condensation derivatives can be generated, depending upon the nature and the molar ratio of the reactants. The results previously obtained can be rationalized[1-3] if the reaction is assumed to involve first an intermediate of type **I**.

$$(1/n)(R_2SnO)_n + HOOCR' \rightarrow R_2Sn(OH)(OOCR')$$
I

Intermediate **I** can either react with another $R_2Sn(OH)(OOCR')$ molecule, yielding a tetraorganodistannoxane 2:2 adduct.

$$R_2Sn(OH)(OOCR') + (R'COO)(HO)SnR_2 \rightarrow R_2(R'COO)SnOSn(OOCR')R_2 + H_2O$$
2:2 adduct

that usually dimerizes[1]

$$2R_2(R'COO)SnOSn(OOCR')R_2 \rightarrow [R_2(R'COO)SnOSn(OOCR')R_2]_2$$
II, dimer of the 2:2 adduct

or reacts with a second equivalent of R′COOH, yielding

* To whom correspondence should be addressed at AOSC and HNMR, Vrije Universiteit Brussel, Room 8G 508, Pleinlaan 2, B-1050 Brussels, Belgium.
† High Resolution NMR Centre, Free University of Brussels, VUB.
‡ Department of General and Organic Chemistry of the Faculty of Engineering, Free University of Brussels, VUB.
§ Free University of Brussels, ULB.
∥ Present address: Chemistry Department, Faculty of Sciences, University of Tétouan, Tétouan, Morocco.
⊥ The University of Adelaide.
△ Catholic University of Louvain.
○ Martin-Luther University.
⊛ Abstract published in *Advance ACS Abstracts*, February 1, 1994.
(1) (a) Bouâlam, M.; Willem, R.; Biesemans, M.; Mahieu, B.; Meunier-Piret, J.; Gielen, M. *Main Group Met. Chem.* **1991**, *14*, 41. (b) Narula, S. P.; Bharadwaj, S. K.; Sharma, H. K.; Mairesse, G.; Barbier, P.; Nowogrocki, G. *J. Chem. Soc., Dalton Trans.* **1988**, 1719.
(2) (a) Meriem, A.; Willem, R.; Meunier-Piret, J.; Biesemans, M.; Mahieu, B.; Gielen, M. *Main Group Met. Chem.* **1990**, *13*, 167. (b) Tiekink, E. R. T.; Sandhu, G. K.; Verma, S. P. *Acta Crystallogr.* **1989**, *C45*, 1810. (c) Sandhu, G. K.; Sharma, N.; Tiekink, E. R. T. *J. Organomet. Chem.* **1989**, *371*, C1. (d) Chandrasekhar, V.; Day, R. O.; Holmes, J. M.; Holmes, R. R. *Inorg. Chem.* **1988**, *27*, 958. (e) Lockhart, P.; Davidson, F. *Organometallics* **1990**, *6*, 2471. (f) Sandhu, G. K.; Gupta, R.; Sandhu, S. S.; Parish, R. V. *Polyhedron* **1985**, *4*, 81.
(3) (a) Gielen, M.; El Khloufi, A.; Biesemans, M.; Mahieu, B.; Willem, R. *Bull. Soc. Chim. Belg.* **1992**, *101*, 243. (b) Bouâlam, M.; Willem, R.; Biesemans, M.; Gielen, M. *Appl. Organomet. Chem.* **1991**, *5*, 497. (c) Meriem, A.; Willem, R.; Biesemans, M.; Mahieu, B.; de Vos, D.; Lelieveld, P.; Gielen, M. *Appl. Organomet. Chem.* **1991**, *5*, 195. (d) Meriem, A.; Biesemans, M.; Willem, R.; Mahieu, B.; de Vos, D.; Lelieveld, P.; Gielen, M. *Bull. Soc. Chim. Belg.* **1991**, *100*, 367. (e) Bouâlam, M.; Biesemans, M.; Meunier-Piret, J.; Willem, R.; Gielen, M. *Appl. Organomet. Chem.* **1992**, *6*, 197.
(4) Johnson, C. K. ORTEP, Report ORNL-5138. Oak Ridge National Laboratory: Oak Ridge, TN, 1976.

0276-7333/94/2313-1098$04.50/0

Table 1. Fractional Atomic Coordinates (×10⁴) with Esd's in Parentheses

	x/a	y/b	z/c
Sn1	1873(1)	6105(1)	7327(1)
Sn2	2198(1)	7893(1)	5987(1)
Sn3	2927(1)	7702(1)	8488(1)
O30	2327(5)	7205(6)	7298(8)
O40	2753(6)	8557(7)	7216(9)
C1	934(9)	6160(10)	4202(14)
C2	1327(9)	6809(10)	4482(14)
C3	1351(9)	7401(10)	3716(16)
C4	975(11)	7384(13)	2675(16)
C5	580(11)	6729(15)	2413(17)
C6	566(9)	6159(12)	3162(16)
C7	839(10)	5496(12)	4846(16)
N8	1095(8)	5383(8)	5836(14)
O9	933(7)	4683(7)	6279(12)
O10	1683(6)	6868(6)	5426(9)
C11	1622(9)	5312(10)	9947(17)
C12	1361(11)	4884(11)	9028(15)
C13	848(10)	4368(11)	9128(19)
C14	602(12)	4265(13)	10120(22)
C15	833(12)	4665(14)	11043(20)
C16	1358(11)	5202(12)	11008(17)
C17	2148(9)	5848(11)	9931(14)
N18	2351(7)	6171(8)	9071(12)
O19	2883(6)	6617(7)	9278(9)
O20	1619(6)	4964(6)	8065(10)
C21	959(7)	6585(10)	7638(16)
C22	990(9)	7149(12)	8591(18)
C23	375(10)	7615(12)	8662(19)
C24	376(12)	8191(15)	9618(21)
C25	2575(9)	5500(10)	6539(16)
C26	3285(10)	5716(12)	6883(16)
C27	3771(10)	5235(14)	6257(21)
C28	4481(11)	5504(19)	6603(25)
C29	2967(10)	7851(13)	4893(17)
C30	3018(12)	7109(15)	4246(20)
C31	3577(13)	7129(19)	3551(22)
C32	3618(15)	6387(19)	2913(24)
C33	1383(10)	8618(12)	5950(18)
C34	1600(18)	9385(18)	5260(38)
C35	1190(22)	9884(23)	4901(41)
C36	725(15)	9737(24)	4068(35)
C37	3933(9)	7654(13)	8300(18)
C38	4333(10)	7122(15)	9094(21)
C39	4254(13)	7251(16)	10275(24)
C40	4467(14)	8108(21)	10615(21)
C41	2480(10)	8405(12)	9651(17)
C42	2521(18)	8147(23)	10757(23)
C43	2212(19)	8822(23)	11612(27)
C44	2612(19)	9445(25)	11731(34)

a 1:2 adduct[2]

$$R_2Sn(OH)(OOCR') + R'COOH \rightarrow R_2Sn(OOCR')_2 + H_2O$$

III, 1:2 adduct

When the 1:2 adduct **III** is reacted with diorganotin oxide, the dimer of the 2:2 adduct **II** is again generated.[1-3] Whether the end product **II** or **III** is generated depends primarily on the molar ratio 1:1 or 1:2 of the reactants R_2SnO and R'COOH, respectively. In the present paper we report our detailed structural studies on a novel type of condensation product **1**, obtained from salicylaldoxime and di-*n*-butyltin oxide, in which the salicylaldoxime and the di-*n*-butyltin moieties appear in the ratio 2:3. A preliminary communication on this compound, which exhibits antitumor activity, was already presented.[3e]

Results

Synthesis. In contrast to the substances **II** and **III** above, our new complex of salicylaldoxime with di-*n*-butyltin oxide crystallizes in a 2:3 molar ratio, independent of the molar ratio (1:1, 2:3, or 1:2) with which the salicylaldoxime ligand HON=CHC_6H_4OH and di-*n*-butyltin oxide are allowed to react. Elemental analysis and X-ray structure determination reveal that the new compound **1**, as obtained after recrystallization from *n*-hexane, obeys the formula [$(Bu_2Sn)(Bu_2SnO)(Bu_2SnOH)$-(HONZO)(ONZO)], where HONZO represents the HON=CHC_6H_4O- salicylaldoximate residue derived from salicylaldoxime, represented accordingly as HONZOH, and ONZO represents -ON=CHC_6H_4O-. With this representation, **1** is generated according to the stoichiometric equation

$$(3/n)(Bu_2SnO)_n + 2HONZOH \rightarrow \underset{\mathbf{1}}{[(Bu_2Sn)(Bu_2SnO)(Bu_2SnOH)(HONZO)(ONZO)]} + H_2O$$

Table 2. Selected Interatomic Distances (Å) and Angles (deg) with Esd's in Parentheses

O10–Sn1	2.68(1)	C7–C1	1.42(3)
O20–Sn1	2.26(1)	C3–C2	1.40(3)
O30–Sn1	2.14(1)	O10–C2	1.33(2)
N8–Sn1	2.67(1)	C4–C3	1.45(3)
N18–Sn1	2.29(1)	C5–C4	1.43(3)
C21–Sn1	2.15(2)	C6–C5	1.35(3)
C25–Sn1	2.10(2)	N8–C7	1.30(3)
O30–Sn2	2.00(1)	O9–N8	1.39(2)
O40–Sn2	2.17(1)	C12–C11	1.42(3)
O10–Sn2	2.17(1)	C16–C11	1.46(3)
C29–Sn2	2.18(2)	C17–C11	1.45(3)
C33–Sn2	2.12(2)	C13–C12	1.41(3)
O30–Sn3	2.04(1)	O20–C12	1.34(2)
O40–Sn3	2.17(1)	C14–C13	1.37(4)
O19–Sn3	2.13(1)	C15–C14	1.38(4)
C37–Sn3	2.15(2)	C16–C15	1.45(3)
C41–Sn3	2.15(2)	N18–C17	1.29(2)
C2–C1	1.42(3)	O19–N18	1.37(2)
C6–C1	1.44(3)		
O10–Sn1–O30	65.2(4)	C29–Sn2–O30	114.4(6)
O10–Sn1–N8	66.2(7)	C29–Sn2–O40	93.5(6)
O20–Sn1–N8	73.1(7)	C33–Sn2–O10	95.8(6)
O20–Sn1–N18	76.7(5)	C33–Sn2–O30	115.5(7)
N18–Sn1–O30	78.9(4)	C33–Sn2–O40	95.0(7)
C21–Sn1–O10	83.6(6)	C33–Sn2–C29	129.8(8)
C21–Sn1–O20	91.6(6)	O19–Sn3–O30	84.5(4)
C21–Sn1–O30	93.5(5)	O19–Sn3–O40	157.9(4)
C21–Sn1–N8	78.3(6)	O40–Sn3–O30	73.5(4)
C21–Sn1–N18	98.5(6)	C37–Sn3–O19	95.3(7)
C25–Sn1–O10	84.9(6)	C37–Sn3–O30	117.7(7)
C25–Sn1–O20	86.5(6)	C37–Sn3–O40	93.5(7)
C25–Sn1–O30	96.4(6)	C41–Sn3–O19	99.6(7)
C25–Sn1–N8	82.2(6)	C41–Sn3–O30	116.0(6)
C25–Sn1–N18	100.4(6)	C41–Sn3–O40	91.6(6)
C25–Sn1–C21	160.0(7)	C41–Sn3–C37	125.3(8)
O10–Sn2–O30	78.3(4)	Sn1–O30–Sn2	121.0(5)
O10–Sn2–O40	152.6(4)	Sn3–O30–Sn1	128.1(5)
O40–Sn2–O30	74.3(4)	Sn3–O30–Sn2	110.9(5)
C29–Sn2–O10	98.8(6)	Sn3–O40–Sn2	100.7(5)

Solid-State Structure Determination by X-ray Diffraction Analysis. A single crystal of **1** was studied by X-ray diffraction. Fractional atomic coordinates are listed in Table 1, a view of the molecular structure is shown in Figure 1, and selected interatomic parameters are listed in Table 2. Experimental details are given in the Experimental Section in Table 7.

The structure is trinuclear with three *n*-Bu_2Sn centers and features one uninegative salicylaldoximate ligand, i.e. HONZO, defined by atoms C1 to O10, and one dinegative ligand, i.e. ONZO, with the C11 to O20 atoms, each of

(5) (a) Christofides, J. C.; Davies, D. B.; Martin, J. A.; Rathbone, E. B. *J. Am. Chem. Soc.* **1986**, *108*, 5738. (b) Christofides, J. C.; Davies, D. B. *J. Am. Chem. Soc.* **1983**, *105*, 5099. (c) Akitt, J. W.; Howarth, O. W. *J. Chem. Soc., Faraday Trans. 1* **1989**, *85*, 121.

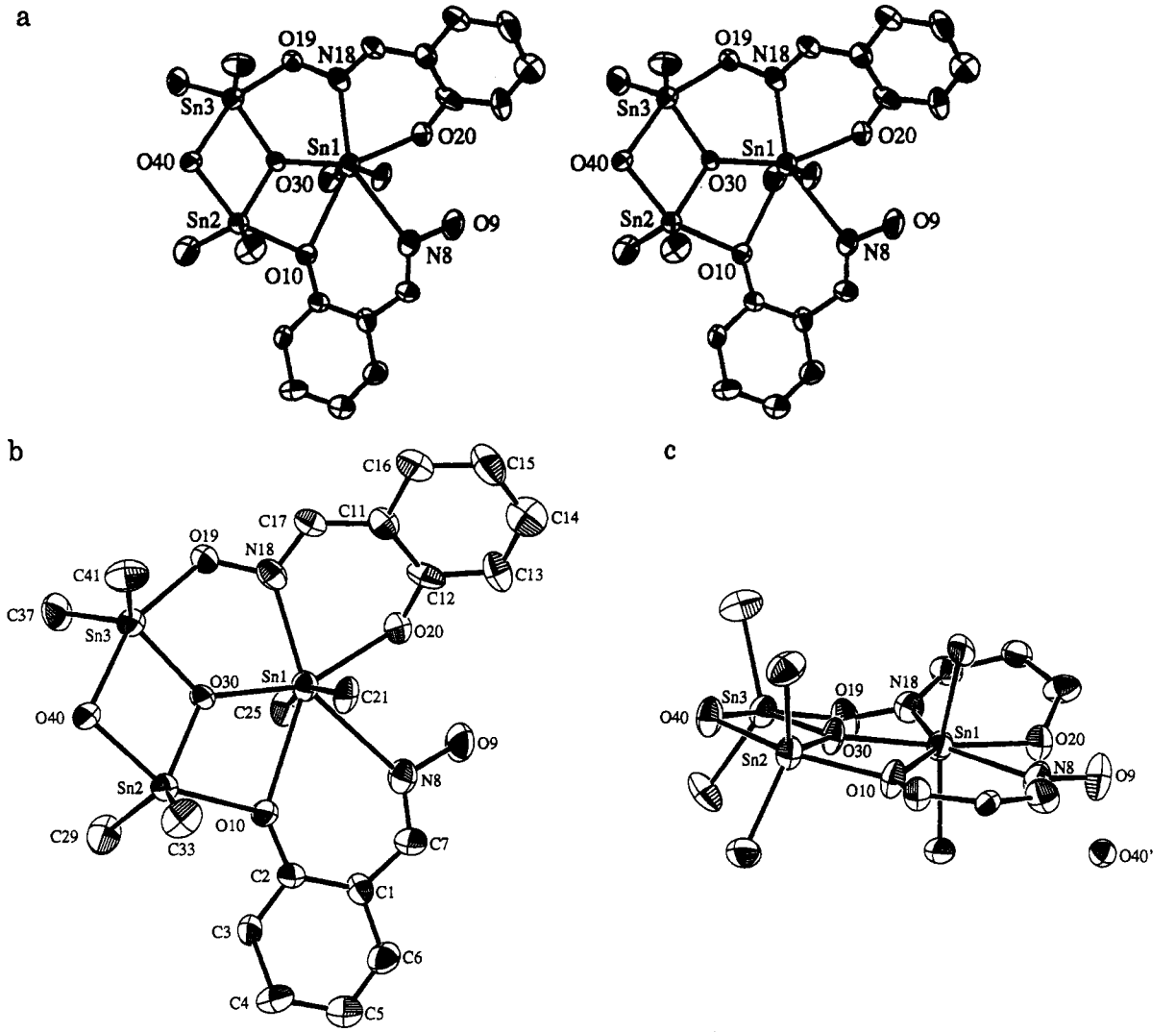

Figure 1. Molecular structure[4] of compound 1 (for reasons of clarity only the C_α carbon atoms of the butyl groups are shown): (a) stereoview of the molecule; (b) the numbering scheme employed; (c) profile view showing the relative disposition of a symmetry-related O40′ atom to the molecule (see text).

which coordinates in the tridentate mode. The central Sn1 atom exists in a distorted-pentagonal-bipyramidal geometry with the *n*-Bu groups occupying axial positions, the bond angle C21–Sn1–C25 being 160.0(7)°. The pentagonal plane is defined by the N18 and O20 atoms of the ONZO ligand, the N8 and O10 atoms of the HONZO ligand, and the O30 atom, which simultaneously bridges the Sn2 and Sn3 atoms and hence is three-coordinate. The pentagonal plane, containing the Sn1 atom, is planar to ±0.04 Å. The N8 and O10 atoms coordinate the Sn1 atom at considerably longer distances of 2.67(1) and 2.68(1) Å, respectively, compared with the Sn1–N18 and Sn1–O20 distances of 2.29(1) and 2.26(1) Å, which is consistent with the higher negative charge on the ONZO ligand, i.e. deprotonation at the O19 atom. Although the longer Sn–L distances are longer than the sum of the covalent radii of the respective atoms, they must be considered as bonding interactions. In contrast to the seven-coordinate Sn1 atom, the Sn2 and Sn3 atoms exist in distorted-trigonal-bipyramidal coordination geometries. The Sn2 and Sn3 atoms are linked via the tricoordinate O30 atom, which also coordinates the Sn1 atom, and by a symmetrical hydroxyl bridge at O40.

The hydrogen atoms were not located in the structure analysis, and hence the location of the hydroxyl proton is open to some conjecture; i.e., does this atom reside on the O19 or O40 atom? Support for the hydroxyl proton being at the O40 atom in the crystalline state is indirect but conclusive (see Discussion).

The two salicylaldoxime moieties exhibit highly inequivalent bonding schemes. In the first ligand (A, HONZO, from C1 to O10) the phenolate oxygen O10 is bound to Sn2, and the aldoxime oxygen O9 is uncoordinated. In the second ligand (B, ONZO, from C11 to O20), the O20 and N18 atoms chelate the tin atom Sn1 and the N18–O19 atom group of the aldoximate bridges Sn1 to Sn3. The ligand A is nearly planar, with Sn1 and Sn2 coplanar. In contrast, ligand B is dramatically twisted, since the atom N18 is 0.31 Å away from the mean plane of the aromatic ring it is associated with.

Mössbauer Spectroscopy. The Mössbauer spectrum of compound 1 is compatible with the existence of two types of tin sites present in the approximate ratio of 70:30 with respective isomer shifts of 1.06 and 1.68 mm/s and quadrupole splittings of 2.96 and 3.48 mm/s relative to $Ca^{119m}SnO_3$. These data are in complete agreement with the structure determined by X-ray diffraction, the former quadrupole splitting lying in the value range typical for five-coordinate tin atoms and the latter being in agreement with the seven-coordinate tin atom.

Solution-State Studies by NMR Spectroscopy. 1D Spectra. The standard ^1H NMR spectrum of compound 1 in C_6D_6 reveals numerous resonances with high and low intensities. While the low-intensity resonances are dif-

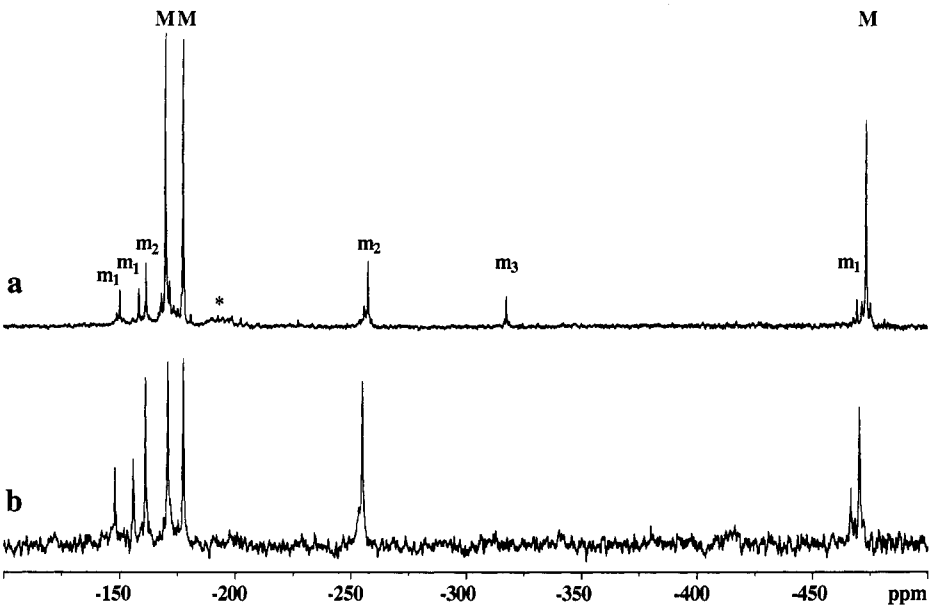

Figure 2. (a) ^{119}Sn NMR spectrum of a sealed sample of 1 in $CDCl_3$ solution recorded at room temperatures (b) ^{119}Sn NMR spectrum of 1 recorded at room temperature after heating the sample for 48 h at 55 °C and cooling it to room temperature. The asterisk denotes a resonance from an unidentified trace species.

Table 3. ^{119}Sn Resonances of the Major Species M and the Three Minor Species m_1, m_2, and m_3 in $CDCl_3$ and C_6D_6 Solution[a]

		species			
	tin atom	M	m_1	m_2	m_3
$CDCl_3$	Sn1	−473.9 [362/346] [55] {*1028*}	−469.6 [290] [38]	−257.5 [289/271] [131] [27][b]	−318.3 [185][b]
	Sn2	−177.6 [68] [57] {*634*}	−158.3 [108] [38] {*594*}	−161.3 [293/274] [128]	
	Sn3	−170.2 [362/345] [69] {*630*}	−150.2 [309/296] [110] {*600*}		
C_6D_6	Sn1	−471.5 [366] [60] {*1031*}	−467.2 [~300] [40]	−255.4 [~284] [130]	−315.4 [196][b]
	Sn2	−177.5 [74] [59] {*638*}	−156.0 [112] [38]	−160.9 [287] [131]	
	Sn3	−171.1 [370] [75] {*633*}	−148.2 [306] [114]		

[a] Chemical shifts are given in ppm with respect to 10% tetramethyltin in $CDCl_3$ or C_6D_6 taken as external reference, $^nJ(^{119}Sn–^{119/117}Sn)$ coupling constants in Hz are given in brackets; $^1J(^{119}Sn–^{13}C)$ values in Hz are given in italics and enclosed by braces. [b] $^2J(^{119}Sn–^{117}Sn)$.

ficult to analyze, several characteristics are to be outlined for the high-intensity patterns. First, the methyl region of the butyl groups reveals three equally intense triplets at 0.80, 0.88, and 0.96 ppm. Second, all the aromatic multiplet patterns expected for the oxime ligand appear duplicated. Likewise, two singlets are observed for the oxime proton at 8.22 and 8.36 ppm. These observations evidence the existence in solution of a major species, M, containing three inequivalent di-*n*-butyltin and two inequivalent salicylaldoxime moieties, as in the solid-state structure.

The ^{119}Sn NMR spectra shed some light into the origin of the low-intensity resonances of the ^1H spectrum and confirm the observations made for the highly populated species M. Figure 2 displays two complete ^{119}Sn NMR spectra recorded at 93.2 MHz of compound 1 in $CDCl_3$ solution. The spectrum of Figure 2a was obtained at room temperature. The spectrum of Figure 2b was obtained likewise at room temperature; however, it was acquired after the sample was heated to 55 °C for 48 h and then cooled to room temperature prior to data acquisition. After 5 days, the initial spectrum is restored within experimental error, showing the chemical changes achieved upon heating to be reversible.

Table 3 gives an overview of the chemical shift and scalar coupling data obtained at room temperature from the ^{119}Sn NMR spectra of compound 1 in $CDCl_3$ and C_6D_6 solutions. They provided identical resonance patterns within 3 ppm. Figure 2 as well as Table 3 reveals the presence of three highly and equally intense resonances, assigned to the major species M, and of six resonances with various intensities, at most 20% of a ^{119}Sn resonance of M. The $^nJ(^{119}Sn–^{119/117}Sn)$ coupling patterns allow us to identify these six minor resonances as a set of three equally intense resonances of a minor species m_1, a pair of two equally intense resonances of a second minor species m_2, and a single resonance of a third species, m_3.

Figure 3 provides spectral expansions of ^{119}Sn NMR spectra recorded at 93.2 MHz in $CDCl_3$ solution from three samples having undergone different chemical preparations prior to acquisition. Thus, sample preparation was achieved so as to make optimal observation of the satellites of all species possible. The spectrum of M and m_3 was obtained from the standard equilibrum mixture at room temperature. The spectrum of m_2 was recorded after preheating the sample at 55 °C followed by rapid cooling to room temperature. Last, the spectrum of m_1 was obtained from the crude reaction mixture of a 1:1 condensation of salicylaldoxime and di-*n*-butyltin oxide in refluxing toluene/ethanol. Indeed, it turned out that, when this reaction mixture is rapidly evaporated to dryness, the crude solid isolated without crystallization was almost pure m_1 with only traces of M and free salicylaldoxime.

The species M and m_1 exhibit very similar ^{119}Sn spectral features. They each have two resonances in the range −150 to −180 ppm, one resonance at much higher field around −470 ppm, and very similar $^nJ(^{119}Sn–^{119/117}Sn)$ coupling patterns, revealing that each tin atom is coupled to the two other tin atoms. Both resonances of species m_2, at −161 and −258 ppm, exhibit each two pairs of $^nJ(^{119}Sn–^{119/117}Sn)$ satellites in $CDCl_3$ at 289/271 and 131 Hz

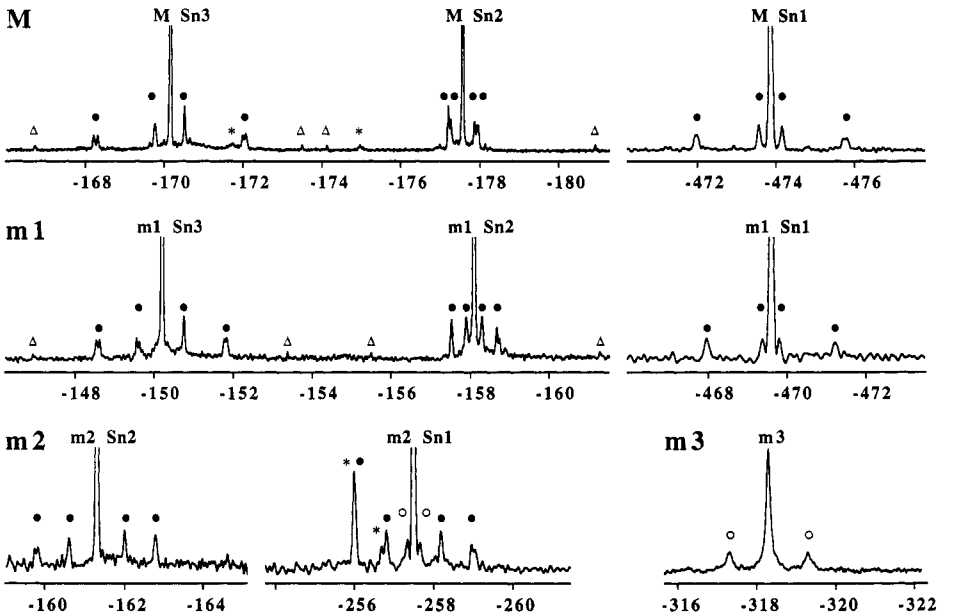

Figure 3. Spectral expansions of three ^{119}Sn NMR spectra recorded at 93.2 MHz for 1 in $CDCl_3$ solution at room temperature. The spectra of the species M and m_3 were recorded with the room-temperature equilibrum mixture. The spectrum of the species m_1 was recorded with the 1:1 reaction mixture. The spectrum of m_2 was recorded after preheating the sample at 55 °C and cooling it rapidly to room temperature. Gaussian resolution enhancement was used with various parameters according to the observed line widths. Solid dots represent $^nJ(^{119}Sn-^{119/117}Sn)$ coupling satellites, open circles represent $^nJ(^{119}Sn-^{117}Sn)$ coupling satellites, open triangles represent $^1J(^{119}Sn-^{13}C)$ satellites, and asteriks represent resonances from unidentified further minor species. The main resonances of M, m_1, and m_2 are vertically out of scale. M, m_1, m_2, and m_3 represent the four species observed at room temperature, as identified from the spectral data (see text).

(unresolved), while the resonance at higher field exhibits an additional pair of $^nJ(^{119}Sn-^{117}Sn)$ coupling satellites of 27 Hz. Finally, the single resonance of m_3 at −318 ppm exhibits a pair of broad satellites with a J splitting of 185 Hz and an intensity of *ca.* 20–25% of the total intensity.

The interconnection between the ^{119}Sn resonances, as deduced from these coupling data, is confirmed by the spectrum of Figure 2b, which merely reflects the chemical composition of 1 in solution above 55 °C with the NMR spectral characteristics at room temperature. The single resonance of m_3 is the only one that disappears into the noise. Both resonances of m_2 have dramatically and simultaneously increased in intensity. The three resonances associated with M and m_1 have respectively dramatically decreased and increased, but less markedly than for m_2.

Figure 4 displays three expansions of ^1H NMR spectra of 1 in the spectral area of the C–H proton of the oxime group. Figure 4a is a standard spectrum at room temperature. The spectrum in Figure 4b was likewise obtained at room temperature; however, it was acquired after the sample was preheated for 4 days at 55 °C but largely before the mixture reequilibrated to its composition at room temperature. The spectrum in Figure 4c, which turns out to be identical to Figure 4a within experimental error, confirms the reversibility of the chemical composition changes, as Figure 4c was acquired at room temperature after the sample was allowed to reequilibrate for 1 week to its initial composition.

Figure 5 displays the variation of the intensity of six resonances of oxime C–H protons as a function of time, over a period of *ca.* 20 h, monitored at room temperature, after the sample was heated to 55 °C for 4 days. After this period of 20 h the initial equilibrium signal intensity pattern was far from being restored. Three resonances of comparable intensity decreased only slightly in intensity but did so synchronously. This spectral behavior parallels

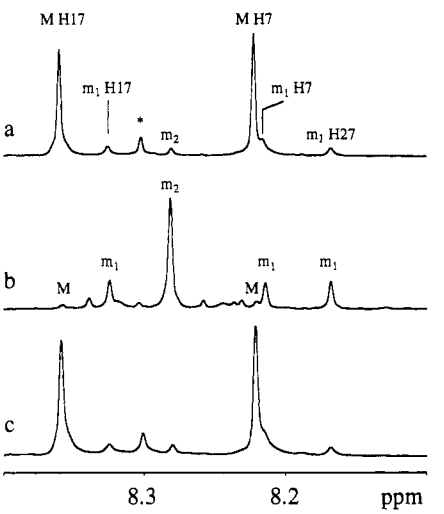

Figure 4. Spectral expansions of the ^1H NMR spectrum of 1 in C_6D_6 solution at room temperature in the resonance area of the C–H proton of the oxime group: (a) standard room-temperature spectrum; b) room temperature spectrum obtained after preheating of the sample for 4 days to 55 °C; (c) room-temperature spectrum after chemical reequilibration for 1 week. The asterisk is used to point out that the oximic C–H proton resonance of m_3 is isochronous with a resonance of an unidentified minor species.

that of the ^{119}Sn resonances of m_1. These resonances are therefore assigned to species m_1 and labeled accordingly in parts a and b of Figure 4. Only two hydroxylic aldoxime proton resonances are observed at 13.93 and 10.90 ppm. They parallel nicely, however, the behavior of the oximic C–H proton resonances of species m1.

Two oximic C–H proton resonances with almost identical intensities increased synchronously. Since they have the resonance frequencies of the major species M in the initial ^1H spectrum and evolve toward their normal high intensity at room temperature, they are unambiguously assigned to

Table 4. Low-Field ^1H Oxime (H7, H17, H27, H_L), Aromatic (H3), and Hydroxylic Proton Resonances Correlated with ^{119}Sn Resonances[a]

M				m_1				m_2			
Sn1	−471.5	H7	8.22 (^3J = 13)	Sn1	−467.2	H7	8.21 (^3J = 13)	Sn1	−255.4	H_L	8.28 (^3J = 39)
		H17	8.36 (^3J < 2)			H17	8.32 (^3J < 2)			H3	6.73 (^4J = 8)
		OH9	13.98 (^3J < 2)			OH9	13.93 (^3J < 2)				
		OH19	~0.9 (broad)								
Sn2	−177.5	H3	6.50 (^4J = 15)	Sn2	−156.0	H3	6.45 (^4J = 15)	Sn2	−160.9	H_L	8.28 (^5J = 3)
		H17	8.36 (^5J < 2)			H17	8.32 (^5J < 2)				
						H27	8.17 (^5J < 3)				
		OH19	~0.9 (broad)			OH29	10.90[b]				
Sn3	−171.1	H17	8.36 (^4J = 4)	Sn3	−148.2	H17	8.32 (^4J = 4)				
						H27	8.17 (^5J < 3)				
		OH19	~0.9 (broad)			OH29	10.90[b]				

[a] Data obtained from the proton detected 2D ^1H–^{119}Sn HMBC spectrum of compound **1** in C_6D_6. Chemical shift data are given in ppm. $^nJ(^1H–^{119}Sn)$ coupling constants are given in Hz and were obtained from F_2 slices of the 2D HMBC spectra presented in Figure 6. The species m_3 has an Sn resonance at −315.4 ppm and an H_L resonance at 8.30 ppm (^3J = 11 Hz). [b] No cross peaks observed.

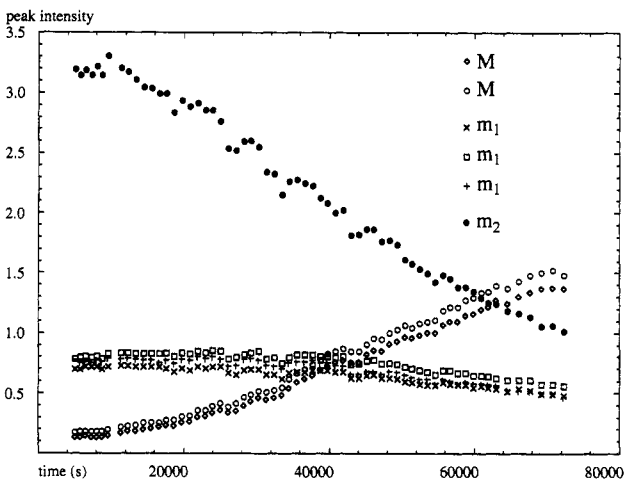

Figure 5. Time evolution of the oxime C–H proton resonances in the species M, m_1, and m_2 after the sample of **1** is heated for 4 days to 55 °C in C_6D_6 and cooled to room temperature prior to time monitoring over a period of *ca.* 20 h.

the species M. They are labeled M H17 and M H7 in parts a and b of Figure 4. For M also, a hydroxylic proton resonance observed at 13.98 ppm parallels the behavior of its oximic C–H proton resonances. In addition, a broad hydroxylic proton resonance, partially hidden by the methyl resonances, is likewise observed for M between 0.80 and 1.00 ppm.

Finally, a last single oximic C–H resonance decreases dramatically as a function of time (Figure 5). As its behavior parallels that of the ^{119}Sn resonances of m_2, it can be assigned to the latter species. Species m_2 does not exhibit any hydroxylic proton resonance.

It should be pointed out that, after heating, other small resonances not visible in the room-temperature equilibrium mixture are observed. Their intensities are, however, too low to deserve any trial of assignment.

Obviously, the three ^{119}Sn resonances and the two intense oxime C–H proton resonances associated with species M strongly suggest the latter to have a structure in solution similar to that in the crystalline state (Figures 1 and 9). However, ^1H and ^{119}Sn SIMPLE-NMR[5] experiments shed some light on the behavior of the OH19/OH40 proton in solution. Secondary isotopic effects on the ^1H chemical shift ($\delta_{^1H^2H} - \delta_{^1H^1H}$) of −0.005 and −0.007 ppm, resulting from the deuteration of the hydroxyl groups, were observed for the oximic C–H protons H7 and H17, respectively. This observation strongly suggests the presence of the hydroxylic proton on the O19 atom. However, the secondary isotopic effects on the ^{119}Sn chemical shift ($\delta_{^{119}Sn^2H} - \delta_{^{119}Sn^1H}$) of +1.408, +1.099, and +1.151 ppm, observed in a ^{119}Sn SIMPLE-NMR experiment for the tin atoms Sn1, Sn2, and Sn3, respectively, are not in agreement with this proposal. Indeed, the secondary isotopic effects on the ^{119}Sn resonances of the Sn2 and Sn3 atoms are of the same order of magnitude. This supports rather the crystalline state structure in which the hydroxylic proton is most likely bound to the O40 atom (see Figure 9 and below in 2D ^1H-^{119}Sn HMBC Spectroscopy and Discussion).

The behavior of the minor species m_1 in the partial deuteration experiments differs from that observed for M. In the ^1H SIMPLE-NMR experiment a secondary isotopic effect is only observed for the oximic C–H proton H7 (−0.005 ppm), while in the ^{119}Sn SIMPLE-NMR spectrum only the Sn1 resonance is shifted (+1.350 ppm).

2D ^1H–^{119}Sn HMBC Spectroscopy. In order to confirm the correlation between the ^{119}Sn resonances and the oxime proton ^1H resonances proposed above for the different species M, m_1, m_2 and m_3, as well as to precisely determine their structure, we performed two-dimensional proton detected ^1H–^{119}Sn heteronuclear multiple bond correlation (2D ^1H–^{119}Sn HMBC) experiments, using the pulse sequence and phase cycling scheme proposed by Bax and Summers.[6] A 2D HMBC provides a two-dimensional map of the chemical shifts of ^{119}Sn nuclei along the F_1 axis and those of ^1H nuclei together with their possible *J*-patterns along the F_2 axis which are correlated to one another through mutual ^1H–^{119}Sn couplings. Such spectra therefore specifically edit ^1H resonances of protons from isotopomers of the compound containing exclusively a ^{119}Sn isotope and coupled to the latter. We recently showed the usefulness of this technique in structural elucidations of organotin compounds.[7]

Table 4 gives an overview of the observed cross peaks with their final assignment.

Figure 6 represents the 2D ^1H–^{119}Sn HMBC spectra in the area of the oxime and aromatic protons, respectively obtained at room temperature from the equilibrium mixture (Figure 6a) and after the sample was heated for 48 h to 55 °C followed by quenching to room temperature prior to aquisition (Figure 6b). Figure 6b yields additional information about the major species present at higher temperature, namely m_1 and m_2.

In order to increase the resolution along the ^{119}Sn F_1 axis, a small spectral window including only the high-field

(6) Bax, A.; Summers, M. F. *J. Am. Chem. Soc.* **1986**, *108*, 2093.
(7) (a) Kayser, F.; Biesemans, M.; Gielen, M.; Willem, R. *J. Magn. Reson.* **1993**, *A102*, 249. (b) Kayser, F.; Biesemans, M.; Pan, H.; Gielen, M.; Willem, R. *J. Chem. Soc., Perkin Trans. 2*, in press.

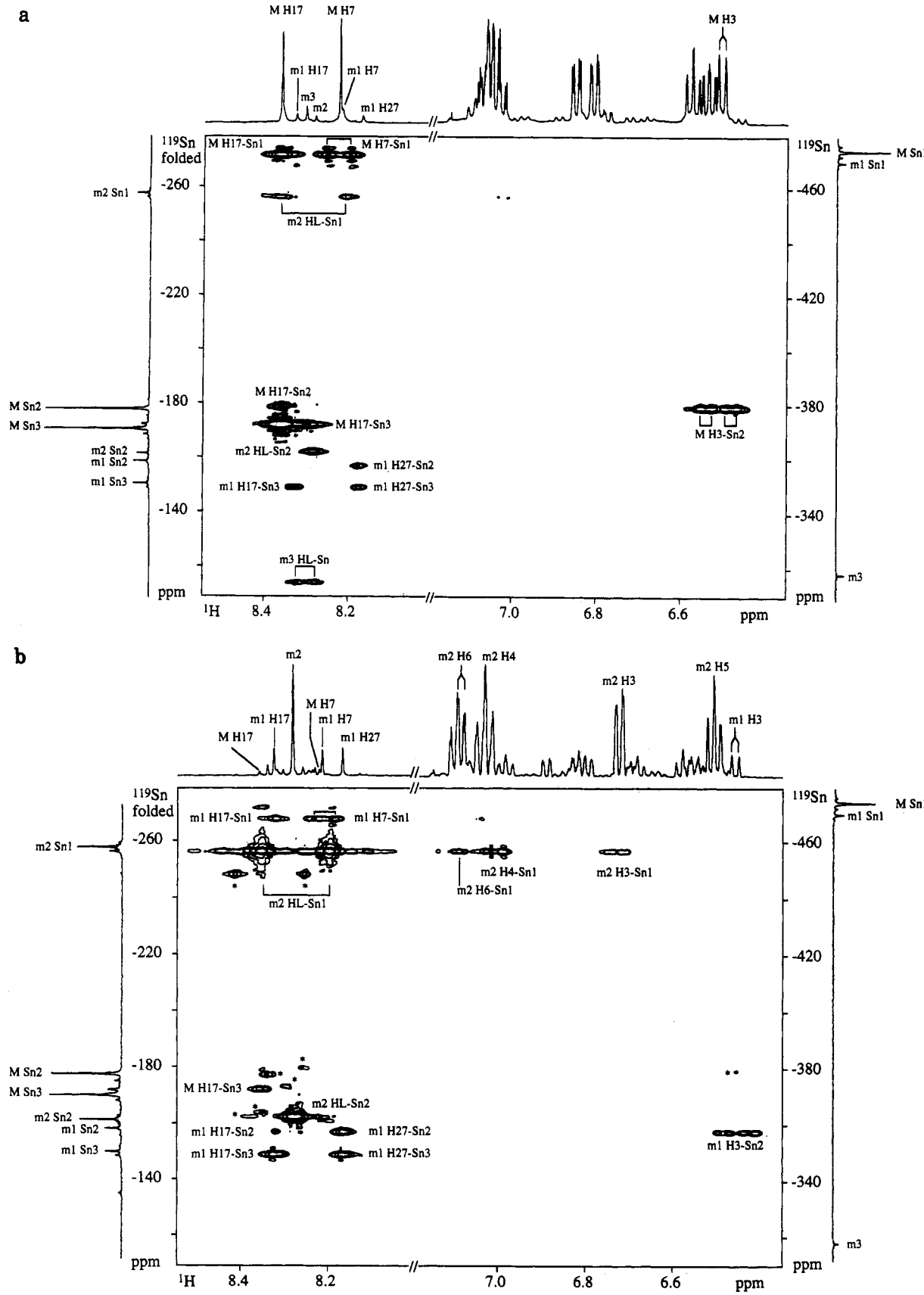

Figure 6. 2D ^{1}H–^{119}Sn HMBC spectra, obtained respectively at 250.13-MHz and at 93.2-MHz ^{1}H and ^{119}Sn frequencies, of compound **1** in C_6D_6 at room temperature (a) from the equilibrium mixture and (b) after heating the sample for 48 h at 55 °C followed by quenching to room temperature prior to acquisition, in the oxime and aromatic proton regions. The spectral window was chosen from −300 to −500 ppm along the ^{119}Sn F_1 axis, resulting in back-folding, into this window, of the resonances between −100 to −300 ppm. The room-temperature equilibrum mixture 1D ^{119}Sn spectrum in the high-field region is shown on the right hand side of the 2D maps and that of the back-folded low-field region on the left-hand side. The 1D ^{1}H spectra obtained at 500.13 MHz corresponding to the mixture at the beginning of the HMBC experiments are given at the top of the 2D maps. The corresponding 1D ^{119}Sn spectra recorded at 93.2 MHz after the HMBC experiments are displayed on the vertical axes. Asterisks denote noise or unidentified minor species.

resonances from −300 to −500 ppm was chosen. This results in back-folding, into this window, of the low-field resonances between −100 and −300 ppm. The spectral window was chosen in such a way that no overlap could occur between the back-folded low-field and the "normal" high-field resonances. Figure 6 shows the standard 1D ^{119}Sn spectrum in the high-field region on the right-hand side of the 2D map and that of the back-folded low-field region on the left-hand side. The standard 1D ^{1}H spectrum is given at the top of the 2D maps.

Figure 6a and Table 4 reveal that the low-field ^{1}H resonance of the major species M at 8.36 ppm exhibits a cross peak with its three ^{119}Sn resonances. In contrast, the high-field ^{1}H resonance of M at 8.22 ppm exhibits a cross peak with only a single ^{119}Sn resonance, that at high field at −474 ppm. Except for the open question of the exact location of the hydroxylic proton on atom O19 or O40, these data readily support the proposal that the major species M in solution and the solid-state compound are identical. Thus, the high-field ^{1}H resonance at 8.22 ppm is assigned to the oxime proton H7, the $^{1}H-^{119}Sn$ correlation appearing as a doublet along the ^{1}H F_2 axis because of a $^{3}J(^{1}H-^{119}Sn)$ coupling through the bond sequence H7–C7–N8–Sn1 (see Figures 1 and 9). The heteronuclear nature of the latter coupling was confirmed by an analogous 2D HMBC experiment performed with ^{119}Sn decoupling during acquisition. No $^{1}H-^{119}Sn$ correlations are observed with the tin atoms Sn2 and Sn3 because these would have to arise from at least $^{5}J(^{1}H-^{119}Sn)$ couplings (*e.g.* H7–C7–N8–Sn1–O30–(Sn2 or Sn3), H7–C7–N8–Sn1–O10–Sn2, H7–C7–C1–C2–O10–Sn2). In contrast, the low-field ^{1}H resonance at 8.36 ppm is assigned to the oxime proton H17. Its $^{1}H-^{119}Sn$ correlation with Sn1 is assigned to a $^{3}J(^{1}H-^{119}Sn)$ coupling through the bond sequence H17–C17–N18–Sn1. The cross peak appears as a singlet because the latter coupling is weaker, probably because the ligand B is twisted out of the mean plane of the molecule. Indeed, a Karplus type relationship might be invoked to explain the difference in magnitude of this ^{3}J coupling.[8] As for the solid-state structure, the simultaneous bondings of O20 and N18 to Sn1 and of O19 to Sn3 are probably responsible for this twist. The last bonding in turn explains the $^{1}H-^{119}Sn$ correlation of the ^{1}H resonance of H17 with the ^{119}Sn resonance at −170 ppm, which is assigned to Sn3, the latter correlation arising from a $^{4}J(^{1}H-^{119}Sn)$ coupling through the bond sequence H17–C17–N18–O19–Sn3. Accordingly, the third, weaker cross peak is assigned to the $^{1}H-^{119}Sn$ correlation H17–Sn2, which can arise from the cumulation of various $^{n}J(^{1}H-^{119}Sn)$ coupling ($n \geq 5$) pathways (H17–C17–N18–Sn1–O30–Sn2, H17–C17–N18–Sn1–O10–Sn2, H17–C17–N18–O19–Sn3–O40–Sn2, H17–C17–N18–O19–Sn3–O30–Sn2).

Of particular interest are also the HMBC cross peaks of the tin nuclei of species M with the hydroxylic proton resonances. OH9 exhibits a sharp resonance at 13.98 ppm correlated only with the Sn1 atom by a $^{3}J(^{1}H-^{119}Sn)$ coupling through the bond sequence H9–O9–N8–Sn1. In contrast, OH19/OH40 displays a broad resonance in the high-field region and correlates with the three tin nuclei. This together with the results from ^{1}H and ^{119}Sn SIMPLE NMR experiments[5] can be rationalized by considering that species M exists in solution as two tautomeric structures, M_a and M_b (Figure 9), related to one another by a fast proton transfer reaction. In this view, the cross-peak between Sn1 and the hydroxylic proton OH19/OH40 arises from a $^{3}J(^{1}H-^{119}Sn)$ coupling through the pathway H19–O19–N18–Sn1 (structure M_b) combined with two $^{4}J(^{1}H-^{119}Sn)$ couplings through the pathways H40–O40–(Sn2 or Sn3)–O–Sn1 (structure M_a). The observed cross-peaks between the Sn2 and Sn3 tin nuclei and the HO19/HO40 proton resonance originate similarly from a combination of various coupling pathways in structures M_a and M_b.

Of major importance also is the cross peak correlating the tin atom Sn2 of M with an aromatic proton at 6.50 ppm. This cross peak can reasonably arise only from a $^{4}J(^{1}H-^{119}Sn)$ coupling with proton H3, through the coupling pathway H3–C3–C2–O10–Sn2. This assignment of H3 was confirmed by comparing the C3 ^{13}C chemical shift of the free ligand and of ligand A, the $^{13}C-^{1}H$ correlation spectrum clearly identifying H3. This assignment is essential, as it serves as a start to the ligand assignment of the aromatic rings A and B through ^{1}H and ^{13}C NMR data, presented below. No such $^{4}J(^{1}H-^{119}Sn)$ coupling of Sn1 with proton H3 through the coupling pathway H3–C3–C2–O10–Sn1 is observed, which can be rationalized by the fact that in the solid state the bond O10–Sn1 is rather long (2.68(1) Å) compared to the Sn2–O10 bond (2.17(1) Å).

For the minor species m_1, the 2D $^{1}H-^{119}Sn$ HMBC spectrum of Figure 6b confirms the existence of three oxime C–H proton resonances. The similarity of the cross-peak patterns of the high-field ^{119}Sn resonances at −474 and −470 ppm for the species M and m_1, respectively, is especially noticeable. The low-field ^{1}H resonance of m_1, at 8.32 ppm, exhibits a coupling pattern similar to that for the low-field ^{1}H resonance of species M; i.e., it is correlated with the high-field ^{119}Sn resonance at −470 ppm as well as the resonances associated with two pentacoordinated tin nuclei. As for species M, one of these two latter couplings appears to be smaller and is associated with the ^{119}Sn resonance at −158 ppm. The midfield ^{1}H resonance of m_1, at 8.21 ppm, correlates likewise with a single ^{119}Sn resonance, the high-field signal at −470 ppm associated with tin atom Sn1. The high-field ^{1}H resonance of m_1, at 8.17 ppm, correlates with two ^{119}Sn resonances, the two low-field signals at −158 and −150 ppm, associated with its tin atoms Sn2 and Sn3 respectively but not with the high-field resonance of the Sn1 atom. As for species M, the HMBC cross peaks between the tin nuclei and the hydroxylic protons, combined with the results of partial deuteration experiments, reveal some structural features of m1. The correlation peak observed between the HO9 resonance at 13.93 ppm and Sn1 is similar to the one observed in species M. In contrast, no correlation peak at all is observed for the second hydroxylic proton resonating at 10.90 ppm.

The single ^{1}H oximic C–H resonance of species m_2 is correlated to the two ^{119}Sn resonances of m_2 with very different coupling values (39 Hz for Sn1 and <2 Hz for Sn2). These data are in agreement with a species m_2 containing only one type of oxime ligand.

Finally, the species m_3 reveals only a single pair of correlated $^{1}H-^{119}Sn$ resonances, a single doublet at 8.30 ppm for the ^{1}H nucleus and a single singlet at −318 ppm for the ^{119}Sn nucleus ($^{n}J(^{1}H-^{119}Sn)$ = 11 Hz).

The complete interpretation of the aliphatic region of the 2D $^{1}H-^{119}Sn$ HMBC spectrum was not attempted, because it is extremely overcrowded and obscured by non-first-order distortions. Nevertheless, the three well-defined $^{5}J(^{1}H-^{119}Sn)$ cross peaks are noteworthy, corre-

(8) Wrackmeyer, B. *Annu. Rep. NMR. Spectrosc.* **1985**, *16*, 73.

Table 5. ^{13}C and ^{1}H Resonances in C_6D_6 of the Major Solution Species M in the Aliphatic Region[a]

group	tin atom	^{13}C	^{1}H
CH_3	Sn1	13.83	0.796
	Sn2	13.76	0.883
	Sn3	13.88	0.964
γ-CH_2	Sn1	26.91	*1.26*
	Sn2	27.23	*1.30*
	Sn3	27.29	*1.44*
β-CH_2	Sn1	29.35	*1.89*
	Sn2	27.97	*1.68*
	Sn3	27.94	*1.76*
α-CH_2	Sn1	34.88 [*1037/988*]	*1.84*
	Sn2	24.55 [*638/608*]	*1.47*
	Sn3	23.03 [*633/604*]	*1.33, 1.45*

[a] Chemical shifts are given in ppm with respect to TMS. The ^{1}H chemical shifts, given in italics, were obtained from a 2D ^{13}C–^{1}H HETEROCOSY experiment. The $^{1}J(^{119/117}Sn$–$^{13}C)$ coupling constants are given in italics within brackets. The anisochrony of the diastereotopic α-CH_2 proton resonances associated with Sn3 should be noted.

lating the ^{119}Sn resonances of M to the ^{1}H resonance of the terminal methyl group of the butyl group to which they are bound. This observation is of interest, as it allows, together with 2D proton detected relayed ^{1}H–^{13}C heteronuclear multiple quantum coherence spectroscopy (^{1}H–^{13}C HMQC-RELAY) data, the assignment of all the ^{1}H and ^{13}C resonances of the butyl groups of the species M.

^{13}C NMR. The ^{13}C spectra of **1** reveal features along the same line as those deduced from the ^{1}H and ^{119}Sn spectra. Table 5 gives ^{13}C and ^{1}H NMR data for the three butyl groups of the major species M in C_6D_6. For the minor species m_1 ^{1}H, ^{13}C and ^{119}Sn spectra were recorded on the nearly pure compound obtained by fast evaporation from the 1:1 reaction mixture, confirming the presence of three ligands and three Bu_2Sn moieties in this species. Being the result of solution chemistry *in situ*, no attempt was made to assign completely the ^{13}C and ^{1}H resonances of the nonisolable minor species m_2 and m_3. Accordingly, the full assignment of species M only was achieved. The correlations between the ^{13}C and ^{1}H chemical shifts of the species M were obtained from a 2D ^{13}C–^{1}H HETEROCOSY experiment,[9,10] which correlates the chemical shifts of mutually bound ^{13}C and ^{1}H nuclei through their $^{1}J(^{13}C$–$^{1}H)$ coupling. The α-CH_2 ^{13}C resonances of M are easily assigned, as they exhibit well-resolved $^{1}J(^{13}C$–$^{119}Sn)$ and $^{1}J(^{13}C$–$^{117}Sn)$ satellites, the former being confirmed by the ^{119}Sn spectra. One of these satellite pairs exhibits a coupling exceeding 1000 Hz and is assigned to the seven-coordinate Sn1 atom, while the other two, of the order of 600 Hz, are characteristic for the five-coordination exhibited by the two other tin atoms in the solid state. The other butyl CH_2 resonances of M, which appeared in both the ^{1}H and ^{13}C spectra within rather narrow spectral windows, were assigned, starting from the associated α-CH_2 and CH_3 ^{13}C resonances, by a 2D proton detected ^{1}H–^{13}C HMQC-RELAY experiment,[11] which correlates the chemical shifts of ^{1}H nuclei to those of ^{13}C nuclei bound to neighboring carbons through their $^{1}J(^{1}H_\alpha$–$^{13}C_\alpha)$–$^{3}J(^{1}H_\alpha$–$^{1}H_\beta)$ coupling pathways. The $^{2}J(^{13}C$–$^{119/117}Sn)$ and $^{3}J(^{13}C$–$^{119/117}Sn)$ coupling satellites of the β- and γ-CH_2 ^{13}C resonances could not be identified because they are not readily distinguishable from the β- and γ-CH_2 ^{13}C resonances of the minor species m_1, m_2, and m_3. They also strongly overlap with those of the major one M.

Table 6. ^{1}H and ^{13}C Resonances in C_6D_6 of the Major Solution Species M in the Aromatic Region[a]

		free salicylaldoxime		
carbon	ligand	exptl (C_6D_6)	calcd	M
1, 1′	$L_A + L_B$	116.9	119.1	119.3, 120.5
2, 2′	$L_A + L_B$	157.5	153.9	161.7, 163.3
3	L_A	117.0	116.0	118.2 (*6.50*; *dd*; *8*, *1*)
3′	L_B			120.5 (*7.04*; *dd*; *7*, *2*)
4	L_A	131.4[b]	131.5	130.9 (*7.06*; *u*)
4′	L_B			132.1 (*7.05*; *u*)
5	L_A	120.0	121.4	117.2 (*6.56*; *ddd*; *8*, *8*, *1*)
5′	L_B			116.8 (*6.53*; *ddd*; *8*, *8*, *2*)
6	L_A	131.0[b]	128.4	135.5 (*6.85*; *dd*; *8*, *2*)
6′	L_B			132.0 (*6.81*; *dd*; *8*, *2*)
7	L_A	152.9		150.4 (*8.22*; *s*)
17	L_B			155.0 (*8.36*; *s*)

[a] Chemical shifts are given in ppm with respect to TMS. The ^{1}H chemical shifts and the multiplicity patterns deduced from the standard 1D spectrum (s = singlet; d = doublet; dd = doublet of doublets; u = unresolved because of overlapping) are given in italics within parentheses. [b] Resonance assignment interchangeable.

The $^{4}J(^{1}H$–$^{119}Sn)$ coupling between the atoms H3 and Sn2 observed in the proton detected 2D ^{1}H–^{119}Sn HMBC spectrum identifies unambiguously the ligand A of M as well as its tin atom Sn2 because no such $^{4}J(^{1}H$–$^{119}Sn)$ coupling can be observed in ligand B toward either Sn2 or Sn3. This in turn allows the assignment of the α-, β-, and γ-CH_2 ^{1}H nuclei to the tin atoms Sn2 and Sn3 they are associated with.

Because no correlation is observed between the aromatic ^{13}C nuclei of the complexed salicylaldoximes and any tin atom, it would not have been possible to assign the salicylaldoxime ligands to those identified as A and B in the solid-state structure determination without the ^{1}H–^{119}Sn HMBC spectrum.

Table 6 gives an overview of the ^{13}C and ^{1}H NMR data of the two complexed salicylaldoxime ligands of the major species M as well as of the free salicylaldoxime ligand in C_6D_6. The basic ^{13}C assignment was achieved from standard decoupled and DEPT ^{13}C spectra, the latter distinguishing quaternary from tertiary carbons, combined with the chemical shift data of free salicylaldoxime. The ^{13}C resonances of the free ligand were assigned from the aromatic ^{13}C chemical shift increment rules.[10] We deduced the increments of the –CH=NOH group to be 3.4, –1.5, 0.3, and 1.6 ppm for the ipso, ortho, meta, and para carbon atoms from the ^{13}C spectrum of benzaldoxime. For the aromatic O—Sn group, the increments of the OH group were used. The assignments within each of the salicylaldoxime ligands A and B of the major species M were performed in an analogous way as for the butyl groups, from the 2D ^{13}C–^{1}H HETEROCOSY[9,10] and the 2D proton detected ^{1}H–^{13}C HMQC-RELAY[11] spectra, exploiting in addition the multiplicity patterns of the aromatic protons. These are doublets for the protons in ortho positions with respect to the –O—Sn and –CH=NOH→Sn groups and doublets of doublets for those in meta positions.

The minor species m_1, m_2, and m_3 display altogether three or four ^{13}C resonances for each type of aromatic carbon, depending on isochrony and/or overlapping with the resonances from the major species. It was checked that none of these small resonances arise from free salicylaldoxime, the resonance frequencies of which differ significantly.

Solution Chemistry. Attempts to isolate any of these

(9) (a) Freeman, R.; Morris, G. A. *J. Chem. Soc., Chem. Commun.* **1978**, 684. (b) Bax, A.; Morris, G. A. *J. Magn. Reson.* **1981**, *42*, 501.
(10) Kalinowski, H.-O.; Berger, S.; Braun, S. *Carbon-13 NMR Spectroscopy*; Wiley: Chichester, U.K., 1988.
(11) Lerner, L.; Bax, A. *J. Magn. Reson.* **1986**, *69*, 375.

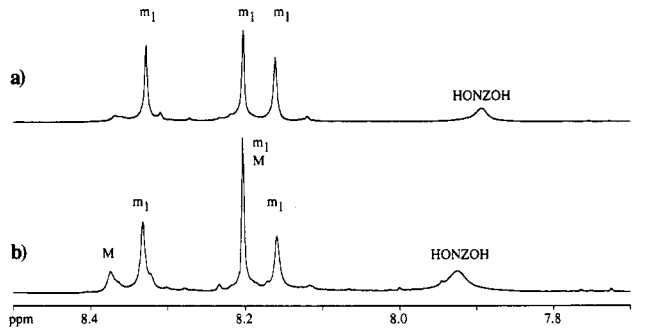

Figure 7. (a) Proton spectrum of the 1:1 molar ratio reaction mixture in C_6D_6 before the addition of water. (b) Proton spectrum of the same sample after addition of water recorded after 1 week.

minor species m_1, m_2, and m_3 either by fractionated recrystallization or by column chromatography on silica or alumina gel, with either chloroform or methylene chloride as eluent, failed, the latter trials giving rise to free salicylaldoxime. We performed the synthesis reaction from molar ratios 1:1, 3:2, and 2:1 of the reactants di-*n*-butyltin oxide and salicylaldoxime, but systematically the compound obtained from each of these three types of experimental initial conditions proved to be **1**, since it provided identical ^1H and ^{119}Sn spectra after isolation and purification by recrystallization in hexane, cyclohexane, or acetonitrile.

However, as stated above, when the 1:1 molar ratio reaction mixture was quickly evaporated and the crude solid redissolved in C_6D_6, it exhibited the ^1H and ^{119}Sn NMR characteristics of the nearly pure m_1 species.

When H_2O is added to a solution of this sample of m_1, species M and free salicylaldoxime ligand are slowly generated (Figure 7b). Thus, species M appears to be a hydrolysis product of the species m_1. Interestingly, when 1 equiv of free salicylaldoxime is added to a solution of M, the spectrum obtained exhibits nearly the same pattern as the spectrum obtained after the hydrolysis of m_1 (compare Figures 7b and 8c). Adding water to a solution of M has no effect at all within a time scale of 1 week.

In a proton spectrum recorded 30 min after the addition of dry zeolite to a solution of **1** in C_6D_6 (Figure 8b) essentially only the resonances of species m_1 and m_2 are observed: the zeolite removes the water from the equilibrum mixture toward the minor species m_1 and m_2.

Species m_2 is favored by an excess of di-*n*-butyltin oxide (Figure 8d). The latter result could be obtained only after heating the sample for 24 h at 60 °C because of the low solubility of the $(Bu_2SnO)_n$ polymer.

Discussion

Solid-State Data. Structures with two types of tin atoms, five-coordinate trigonal bipyramidal and six-coordinate octahedral, were described previously.[1,2] However, in compound **1**, the ratio of the ligand to tin moiety is 2:3 rather than 1:1 or 1:2 as in the former structures. Therefore, besides two five-coordinate tin atoms, an additional tin atom is present. The latter turns out to exhibit seven-coordination. Though still rare, seven-coordination was already reported in several diorganotin derivatives.[12]

Considering that both phenolic functions of the salicylaldoxime molecules have reacted with tin and that the hydrogen atoms were not located in the structure analysis, two possible structures can account for the structure

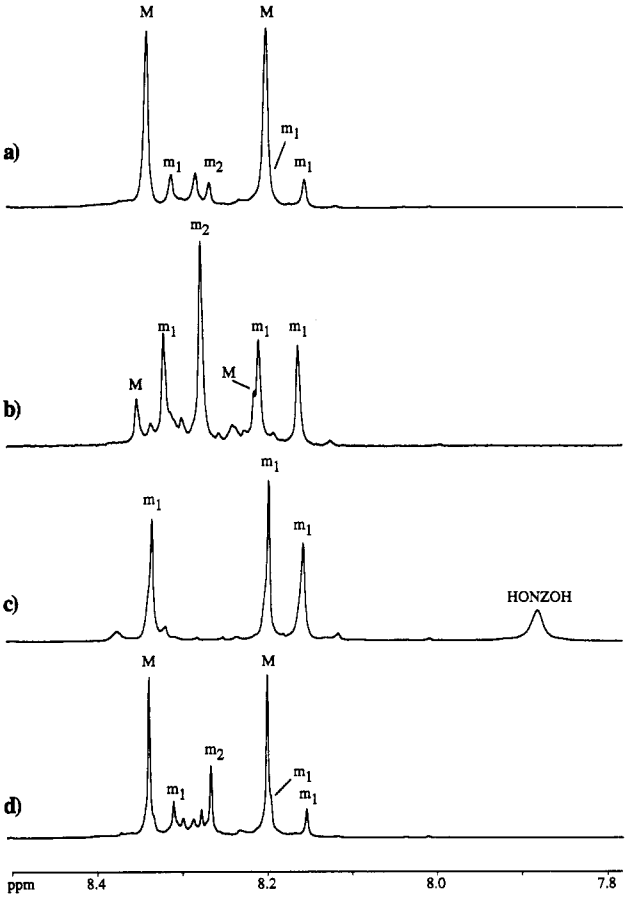

Figure 8. Expansions of the proton spectra in the oximic region (a) of the room-temperature equilibrum mixture in C_6D_6, (b) of this mixture 30 min after the addition of dry zeolite, (c) after the addition of 1 equiv of free salicylaldoxime ligand to the mixture, and (d) after the addition of 1 equiv of Bu_2SnO to the mixture.

displaying the spatial atom arrangement obtained from the X-ray analysis. They are represented in Figure 9 as M_a and M_b. Support for the hydroxyl bridge at the O40 atom, and the solid state structure being M_a, is indirect but highly conclusive.

In the crystal lattice of **1** there is an intermolecular separation of 2.81(2) Å between the O20 and O40′ atoms (symmetry operation: $1.5 - x, -0.5 + y, 1.5 - z$). As the O20 atom is a phenolate oxygen atom, this interaction suggests protonation at the O40 site. The observation that the Sn2– and Sn3–O40 bond distances of 2.17(1) Å are longer than the Sn2– and Sn3–O30 bond distances of 2.00(1) and 2.04 (1) Å, respectively, despite the fact that the O30 atom is bonded to three Sn atoms, is also consistent with the presence of a hydroxyl bridge between the Sn2 and Sn3 atoms. Further, the Sn_2O_2 ring is not planar, with deviations of 0.003(2), 0.003(2), –0.09(1) and 0.11(1) Å for the Sn2, Sn3, O30, and O40 atoms, respectively. This feature is in contrast with normal distannoxane rings. In the trigonal-bipyramidal geometries, the Sn2 atom lies

(12) (a) Gielen, M.; Joosen, E.; Mancilla, T.; Jurkschat, K.; Willem, R.; Roobol, C.; Bernheim, J.; Atassi, G.; Huber, F.; Hoffmann, E.; Preut, H.; Mahieu, B. *Main Group Met. Chem.* **1987**, *10*, 147. (b) Huber, F.; Preut, H.; Hoffmann, E.; Gielen, M. *Acta Crystallogr.* **1989**, *C45*, 51. (c) Gielen, M.; Acheddad, M.; Bouâlam, M.; Biesemans, M.; Willem, R. *Bull. Soc. Chim. Belg.* **1991**, *100*, 743. (d) Gielen, M.; Acheddad, M.; Mahieu, B.; Willem, R. *Main Group Met. Chem.* **1991**, *14*, 73. (e) Swisher, R. G.; Day, R. O.; Holmes, R. R. *Inorg. Chem.* **1983**, *22*, 3692. (f) Lockhart, T. P.; Davidson, F. *Organometallics* **1987**, *6*, 2471. (g) Lockhart, T. P.; Calabrese, J. C.; Davidson, F. *Organometallics* **1987**, *6*, 2479. (h) Meriem, A.; Willem, R.; Meunier-Piret, J.; Biesemans, M.; Mahieu, B.; Gielen, M. *Main Group Met. Chem.* **1990**, *13*, 167.

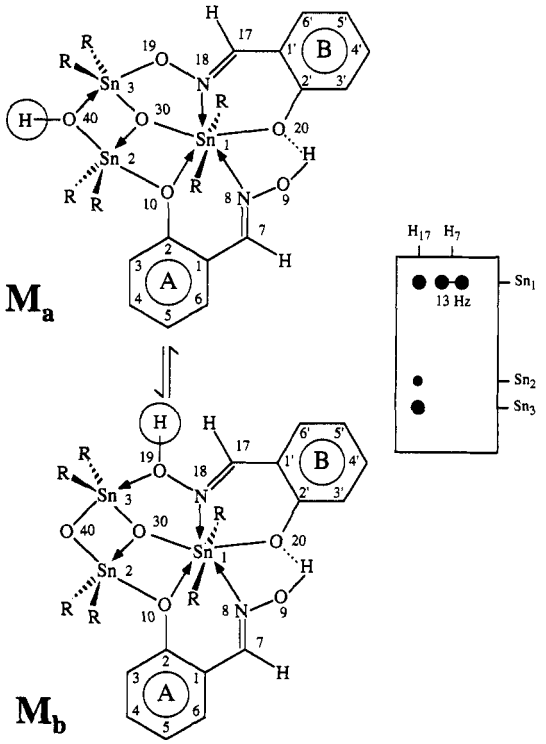

Figure 9. Structure M_a found for compound 1 in the solid state and its tautomer M_b (R = n-butyl). Species M_a and M_b differ only by the location of one hydroxylic proton on respectively O40 and O19. In the solution state, M_a and M_b interconvert on all NMR time scales by proton transfer. A scheme of the ^1H–^{119}Sn coupling pattern observed in the 2D HMBC spectrum in the oximic C–H proton region of M is displayed to the right of the structures.

0.061(2) Å above the trigonal plane in the direction of the O10 atom derived from the phenolate portion of the HONZO ligand A. The distortion from the ideal geometry is greater for the Sn3 atom, which lies 0.125(2) Å above the equatorial plane in the direction of the O19 atom derived from the aldoximate function of the ONZO ligand B. Of interest in the structure are the different coordination modes of the salicylaldoximate ligands.

The O9, O10, N8, C1, C2, and C7 atoms of the uninegative HONZO ligand A are planar to ±0.01 Å, whereas the ONZO ligand B is not planar. In the ONZO ligand the O19–N18–C17–C11 and C17–C11–C12–O20 torsion angles are −176(2) and 1(3)°, respectively, whereas the N18–C17–C11–C12 torsion angle is 19(3)°, indicating a significant twist about the C11–C17 vector. The different ligand geometries reflect the additional steric strain upon coordination of all three donor atoms to tin by the ONZO ligand B in contrast to the HONZO ligand A, which employs two donor atoms only, i.e. the N8 and O10 atoms, in coordination to tin.

The noncoordinating hydroxyl group, O9–H, links both salicylaldoximate residues via an intramolecular hydrogen bond such that the O9···O20 separation is 2.57(2) Å; in the same way, the other ends of the salicylaldoximate ligands can be thought of being linked by a $Bu_2SnO(OH)SnBu_2$ moiety which is bound to the central $Bu_2Sn(HONZO)$-(ONZO) unit. The hydrogen bridge O20···H–O40′ binds two neighboring molecules to one another in the crystal. Figure 10 shows that the structure of 1 differs from those based on a distannoxane motif,[1,2,12] i.e. $\{[R_2SnX]_2O\}_2$ (**A**), where X is a uninegative ligand such as halide or carboxylate. In 1, the cluster network of which is represented by **B**, one of the exocyclic R_2Sn groups bound

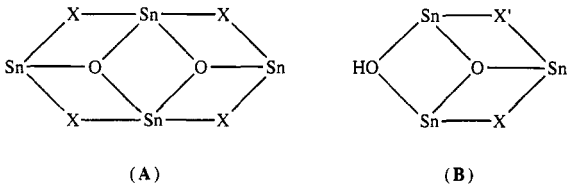

Figure 10. (A) Common tin cluster structures in halides and carboxylates. (B) New cluster type in the present compound 1 (the butyl groups are omitted for clarity).

to the O40 atom has been replaced by a hydrogen atom and X′ represents the dinegative salicylaldoximate ligand.

Solution-State Structures from NMR Data. The ^{119}Sn chemical shifts and the corresponding $^1J(^{13}C$–$^{119/117}Sn)$ coupling constants observed for M are in agreement with the structure found in the solid state containing one seven-coordinate pentagonal-bipyramidal and two five-coordinate trigonal-bipyramidal tin atoms. Our numerous NMR data completely fit into the structure of M given in Figures 1 and 9. The comparison of the ^1H and ^{119}Sn SIMPLE NMR experiment enabled us to locate the hydroxylic OH19/OH40 hydrogen on the O19 *and* the O40 oxygen. Thus, upon substitution of hydroxylic protons for deuterons, the C–H oximic proton resonances of both ligands are almost equally affected. This observation supports M in solution to be M_b with the hydroxylic proton on atom O19. In contrast, the very similar isotopic shifts in the ^{119}Sn resonances of the atoms Sn2 and Sn3 support rather the solid-state structure M_a to exist likewise in solution. Hence, it is proposed that the structures M_a and M_b both exist in solution. The broadness of the resonance of this OH19/OH40 proton in the ^1H spectrum, in strong contrast with the narrow line of the other hydroxylic proton on atom O9, supports the view of M_a and M_b being rapidly interconverting tautomers. The likely basis of this is the easily understood acidity of a proton on either O40 or O19 resulting from the Lewis acidity of the tin atoms Sn2 and Sn3. The intramolecular transfer rate appears to be very fast on the ^1H as well as the ^{119}Sn NMR time scale. In contrast, the very narrow resonance of the hydroxylic proton of O9 supports the view of a highly stable intramolecular hydrogen bridge O9–H···O20 existing as well in solution.

The $^1J(^{13}C$–$^{119/117}Sn)$ coupling constants of *ca.* 600 Hz for the α-CH_2 groups of these five-coordinate tin atoms are in agreement with both butyl groups in equatorial positions of the trigonal bipyramid. In contrast, both the very low value of *ca.* −474 ppm for the ^{119}Sn chemical shift of Sn1 and the very large $^1J(^{13}C$–$^{119/117}Sn)$ coupling constant of *ca.* 1000 Hz[12c,d,13] are in excellent agreement with the Sn1 atom being pentagonal bipyramidal with the two butyl groups occupying the apical positions. Using the $^1J(^{13}C$–$^{119}Sn)$ coupling constant values of Table 3 and the empirical equation proposed by Holeček and Lyčka,[14] the C–Sn–C angles in solution are evaluated to be 178.5, 138.5, and 138.0° for the tin atoms Sn1, Sn2, and Sn3, respectively. They differ somewhat from the values of 160.0(7), 129.8(8), and 125.3(8)° respectively found in the crystalline state.

The 2D ^1H–^{119}Sn HMBC spectrum technique proved to be especially powerful in the assignment of the Sn2 and Sn3 atoms of the structure M. The smaller coupling

(13) (a) Corriu, R. J. P.; Guirin, C. *Adv. in Organomet. Chem.* **1982**, *20*, 265. (b) Gielen, M.; Bouâlam, M.; Biesemans, M.; Mahieu, B.; Willem, R. *Main Group Met. Chem.* **1991**, *14*, 271. (c) Fu, T.; Pan, H.; Willem, R.; Gielen, M. *Bull. Soc. Chim. Belg.* **1990**, *99*, 789.
(14) Holeček, J.; Lyčka, A. *Inorg. Chim. Acta* **1986**, *118*, L15.

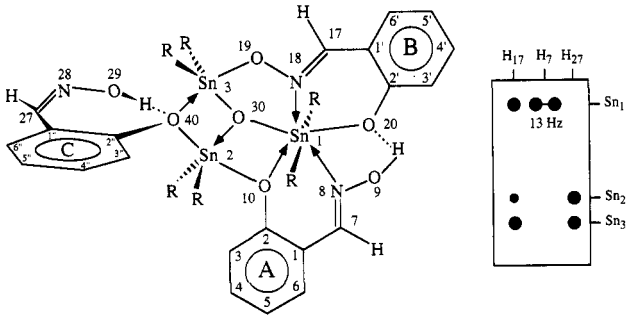

Figure 11. Structure proposed for the minor solution species m_1 (R = *n*-butyl). A scheme of the ^1H–^{119}Sn coupling pattern observed in the 2D HMBC spectrum in the oximic proton region of m_1 is displayed to the right of the structure. The ligand C is proposed to be perpendicular to the plane of the molecule and is probably stabilized by an intramolecular hydrogen bond (see text).

constant of *ca.* 69 Hz associated as satellites with the resonances of the latter atoms obviously arises from the Sn2–O40–Sn3–O30 tin moiety and is therefore a composite of two $^2J(^{119}Sn–O–^{119/117}Sn)$ constants. This coupling is rather small, when compared to the highest value of 240 Hz found in tetraorganodistannoxanes[15] and to the even greater values in some hexaorganodistannoxanes and analogs.[16] We tentatively associate this low value in the present species M with the cyclic strain in the Sn2–O40–Sn3–O30 unit. The higher coupling constant of *ca.* 360 Hz, associated with the tin atoms Sn1 and Sn3, is consistent with ^3J couplings involving the ^{119}Sn nucleus being larger than ^2J ones.[8] Actually, it is likely to be a composite of a $^2J(^{119}Sn–O–^{119/117}Sn)$ coupling involving the Sn1–O30–Sn3 bridge and of a $^3J(^{119}Sn–N–O–^{119/117}Sn)$ coupling from the Sn1–N18–O19–Sn3 moiety. Finally, the presence of a pair of $^2J(^{119}Sn–O–^{119/117}Sn)$ coupling satellites of *ca.* 56 Hz between the tin atoms Sn1 and Sn2 is noteworthy. This coupling is quite small, though comparison of our coupling data with literature data[8] are in any case to be done with caution because all $^nJ(^{119}Sn–^{119/117}Sn)$ coupling satellites result from two potential coupling pathways.

Proposing a structure for the minor species m_1, m_2, and m_3 is more cumbersome, since these species could not be isolated as pure crystalline compounds. Nevertheless, the ^{119}Sn NMR data, with the associated $^nJ(^{119}Sn–^{119/117}Sn)$ coupling patterns, the ^1H resonances of the oximic C–H protons, and especially the proton detected 2D ^1H–^{119}Sn HMBC spectrum correlating the last two types of resonances enable reasonable structures to be proposed for these species.

The very similar 1D ^{119}Sn NMR spectral patterns of the major species M and the minor species m_1 suggest m_1 to display a tin cluster core comparable to that of the major species M. One important difference should however be emphasized: species m_1 involves three rather than two salicylaldoxime ligands, as evidenced unambiguously by the oximic C–H proton resonances (Figure 4), coupled with our time monitoring experiments (Figure 5) and our 2D ^1H–^{119}Sn HMBC spectrum (Figure 6b). Figure 11 proposes a structure for m_1, the bond picture of which accounts for the three different ^{119}Sn resonances as well as for the observed 2D ^1H–^{119}Sn HMBC correlations. In our proposal, the local structures of the three tin atoms of m_1 are basically the same as for species M, as suggested by their very similar ^{119}Sn chemical shifts, $^{119}Sn–^{119/117}Sn$ coupling data, and 2D ^1H–^{119}Sn HMBC cross-peak pattern. The discussion of the 2D HMBC coupling pattern of H7 and H17 of species M applies without any restriction to species m_1. The oximic C–H proton resonance of the third ligand, not present in M, exhibits only 2D HMBC correlations with Sn2 and Sn3. Accordingly, we do not associate the presence of the third salicylaldoxime ligand with the seven-coordinate tin atom but rather with the two five-coordinate ones, the ^{119}Sn chemical shift and coupling data of which indeed differ more significantly from those of M. Obviously, adding the third ligand in m_1 formally just requires the substitution of the O40–H group of M_a for the third ligand C. Indeed, no NMR evidence could be gained for a structure of m_1 with a hydroxylic proton on O19, in contrast to M_b. Thus, a secondary isotopic shift was observed for neither H17 nor Sn2 and Sn3, respectively, in the ^1H and ^{119}Sn SIMPLE NMR experiments. Furthermore, no ^1H–^{119}Sn HMBC cross peak correlating a hydroxylic proton to Sn3 or Sn2 could be detected. In view of this, the O19–Sn3 bond should be of the same type as in M_a. Hence, the structure proposed for species m1 presents a similar bonding scheme for the four-membered–O40–Sn2–O30–Sn3– unit as the one observed for species M except that the third ligand C replaces the O40–H group of M. The absence of any secondary isotopic effect on the Sn2 and Sn3 resonances and the absence of any ^1H–^{119}Sn HMBC cross-peak correlating the HO29 resonance at 10.90 ppm to either of the tin atoms Sn2 and Sn3 are in agreement with such a structure for m_1. In this structure, two likely features supported by experimental data should be outlined. First, the ligand C should be perpendicular to the plane Sn3–O40–Sn2. The identical intensities of the 2D HMBC cross peaks H27–Sn2 and H27–Sn3 are in agreement with this view. Second, as the hydroxylic proton resonance of ligand C at 10.90 ppm is very sharp, in the same way as those around 14 ppm in both M and m_1, the proposed structure is likely to be stabilized by the intramolecular hydrogen bridge O29–H···O40 involving again a nonexchangeable proton.

Indirect support for the structure proposed in Figure 11 for m_1 is provided by the observation that it obeys the formula $[(Bu_2Sn)_2(Bu_2SnO)(HONZO)_2(ONZO)]$, to be compared with that for M, $[(Bu_2Sn)(Bu_2SnO)(Bu_2SnOH)(HONZO)(ONZO)]$. This shows that species M can be generated by hydrolysis from species m_1 by loss of one free salicylaldoxime ligand according to the stoichiometry given in eq 1.

$$m_1 + H_2O \rightleftharpoons M + HONZOH \quad (1)$$

Experimental support for this reaction to occur is given in Figures 7 and 8c. The spectrum in Figure 7a for the 1:1 reaction mixture after fast evaporation shows clearly that almost only m_1 is present. After addition of H_2O the species m_1 hydrolyzes into species M and free salicylaldoxime ligand (Figure 7b). If 1 equiv of free salicylaldoxime ligand is added to a solution containing species M, the equilibrum is displaced toward m_1 (Figures 8a,c).

The ^{119}Sn spectral pattern of m_2 is no longer compatible with the existence of three inequivalent tin atoms. The very peculiar ^{119}Sn NMR spectral pattern of species m_2,

(15) (a) Gielen, M.; El Khloufi, A.; Biesemans, M.; Willem, R. *Appl. Organomet. Chem.* **1993**, *7*, 119. (b) Gielen, M.; Meunier-Piret, J.; Biesemans, M.; Willem, R.; El Khloufi, A. *Appl. Organomet. Chem.* **1992**, *6*, 59. (c) Yano, T.; Nakashima, K.; Otera, J.; Okawara, R. *Organometallics* **1985**, *4*, 1501.

(16) (a) Lockhart, T. P.; Manders, W. F.; Brinckman, F. E. *J. Organomet. Chem.* **1985**, *286*, 153. (b) Lockhart, T. P.; Puff, H.; Schuh, W.; Reuter, H.; Mitchell, T. N. *J. Organomet. Chem.* **1989**, *366*, 61. (c) Puff, H.; Schuh, W.; Sievers, R.; Wald, W.; Zimmer, R. *J. Organomet. Chem.* **1984**, *260*, 271.

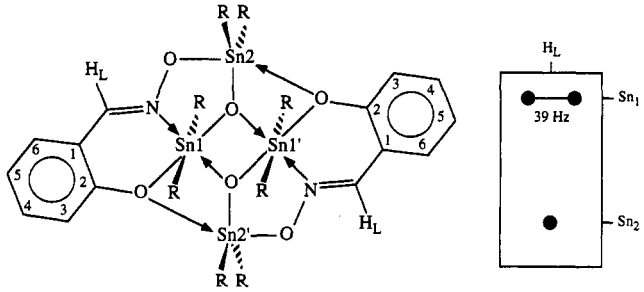

Figure 12. Structure proposed for species m_2 (R = *n*-butyl). A scheme of the ^1H–^{119}Sn coupling pattern observed in the 2D HMBC spectrum in the oximic proton region of m_2 is displayed to the right of the structure.

composed of two equally intense ^{119}Sn resonances each exhibiting two identically split pairs of $^nJ(^{119}Sn$–$^{119/117}Sn)$ coupling satellites and the additional ^{119}Sn–^{117}Sn coupling satellites observed for the high-field resonance (Table 3), leads us to propose the structure shown in Figure 12. Thus, the ^{119}Sn chemical shifts of −161 and −258 ppm are in agreement with the presence of respectively five- and six-coordination for the tin atoms. The two equally intense ^{119}Sn signals are indeed compatible with the two heterotopic pairs of homotopic tin atoms of the structure proposed for m_2 in Figure 12. Moreover, it is easily noticed that each tin atom is coupled to the two neighboring homotopic tin atoms by two heterotopic $^2J(^{119}Sn$–O–$^{119/117}Sn)$ coupling pathways, in excellent agreement with the two pairs of unresolved $^2J(^{119}Sn$–O–$^{119/117}Sn)$ satellites observed. In addition, a small $^2J(^{119}Sn1$–O–$^{117}Sn1')$ is observed. The 2D ^1H–^{119}Sn HMBC cross peaks (Figure 6 and Table 4) are likewise in agreement with the structure proposed, having two equivalent oxime ligands exhibiting a large $^3J(^1H$–$^{119}Sn)$ coupling (39 Hz) between the oximic proton and the Sn1 atom, on the one hand, and a small $^4J(^1H$–$^{119}Sn)$ coupling (3 Hz) between the oximic proton and the Sn2 atom, on the other hand. The very high value for the ^3J coupling could possibly be explained by a Karplus type relationship.[8] Indeed, for the structure proposed in Figure 12 the Sn1←N=C—H_L unit is expected to be planar.

No cross peaks between the Sn2 nucleus and the aromatic proton resonances of the ligand are observed while Sn1 exhibits such couplings. This can be rationalized by the fact that in the proposed structure the coordinative bonds between the phenolic oxygens and the Sn2 atoms are expected to be rather long. The tentative assignment of the aromatic proton resonances of m_2 shown in Figure 6b has been done on the basis of their proton coupling patterns as well as the ^1H–^{119}Sn cross peaks observed in the HMBC spectrum shown in Figure 6b. The resonances of H3 and H6 appear as doublets of doublets arising from one large ortho coupling with H4 and H5, respectively, and one small meta coupling with H5 and H4, respectively. H3 exhibits a rather intense ^1H–^{119}Sn cross peak arising from a $^4J(^1H$–$^{119}Sn)$ coupling through the Sn1–O–C2–C3–H3 bonds. The structure proposed is also in agreement with the absence of hydroxylic proton resonances.

Indirect support for the structure proposed in Figure 12 for m_2 is provided by the observation that it obeys the formula $[(Bu_2Sn)_2(Bu_2SnO)_2(ONZO)_2]$, to be compared with that of M, $[(Bu_2Sn)(Bu_2SnO)(Bu_2SnOH)(HONZO)$-$(ONZO)]$. This shows that species m_2 can formally be generated by reaction of M with 1 equiv of Bu_2SnO accompanied by elimination of water according to the stoichiometry given in eq 2.

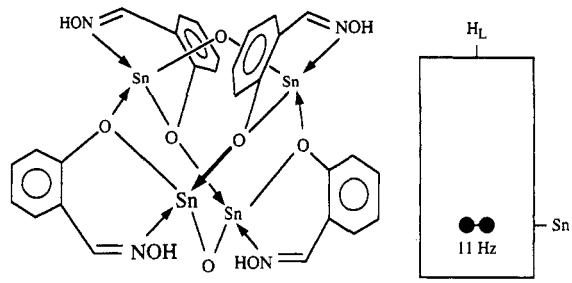

Figure 13. Structure proposed for species m_3. A scheme of the ^1H–^{119}Sn coupling pattern observed in the 2D HMBC spectrum in the oximic proton region of m_3 is displayed to the right of the structure. The *n*-butyl groups have been omitted for clarity.

$$M + Bu_2SnO \rightleftharpoons m_2 + H_2O \quad (2)$$

Experimental support for this reaction to occur is given in Figure 8a,d. If 1 equiv of di-*n*-butyltin oxide is added to a solution containing species M, the equilibrum is displaced toward m_2 (compare parts a and d of Figure 8).

Finally, the species m_3 exhibits a single ^{119}Sn resonance, with, however, unresolved coupling satellites having a total intensity of more than 20% of the complete m_3 ^{119}Sn resonance. This suggests it to be a highly symmetric species containing several symmetry-equivalent tin nuclei each of which is coupled to three other tin atoms through pure $^nJ(^{119}Sn$–O–$^{117}Sn)$ couplings, the $^nJ(^{119}Sn$–O–$^{119}Sn)$ coupling between equivalent ^{119}Sn nuclei being necessarily unobservable. Figure 13 proposes such a structure. Though difficult to visualize, it consists of a bis((salicylaldoximato)di-*n*-butyltin) oxide that dimerizes through a complex network of coordinative O→Sn bonds originating at the phenolic oxygen atoms of the salicylaldoximate moieties, which results in a highly symmetric, adamantane-like cluster. Detailed examination of a Dreiding molecular model reveals this structure (i) to be fairly symmetric, having S_4 symmetry, and (ii) to be realistic from the point of view of ring and bond angle constraints. Its ^{119}Sn chemical shift of −315 ppm is in agreement with the six-coordination proposed. The cross-peak pair correlating the single oximic proton ^1H doublet with the single ^{119}Sn resonance in the 2D ^1H–^{119}Sn HMBC spectrum is likewise in agreement with this proposal, as is the magnitude of the $^3J(^1H$–$^{119}Sn)$ coupling of 11 Hz. The coupling patterns of each tin to its three neighbors are in principle not all identical, since each of the tin atoms is bound to one of its neighbors through a covalent Sn–O–Sn bridge and to two such neighbors by coordinative bonds originating at a trifurcate phenolic oxygen. Henceforth, each tin atom should give rise to two pairs of $^2J(^{119}Sn$–O–$^{117}Sn)$ satellites. This expectation is in agreement with both the significant broadening and the otherwise unexpected high intensities of the satellites actually observed.

The too simple spectral patterns, as well as the lack of more spectral evidence, make this proposal somewhat speculative. Nevertheless, the species m_3 obeys the formula $[(Bu_2Sn)_2(Bu_2SnO)_2(HONZO)_4]$ and it can be accounted for by a reaction involving only the elimination of one Bu_2SnO unit from M:

$$M \rightleftharpoons m'_3 + Bu_2SnO \quad (3)$$

$$2\,m'_3 \rightleftharpoons m_3 \quad (4)$$

where m'_3 represents the monomeric distannoxane giving rise to m_3.

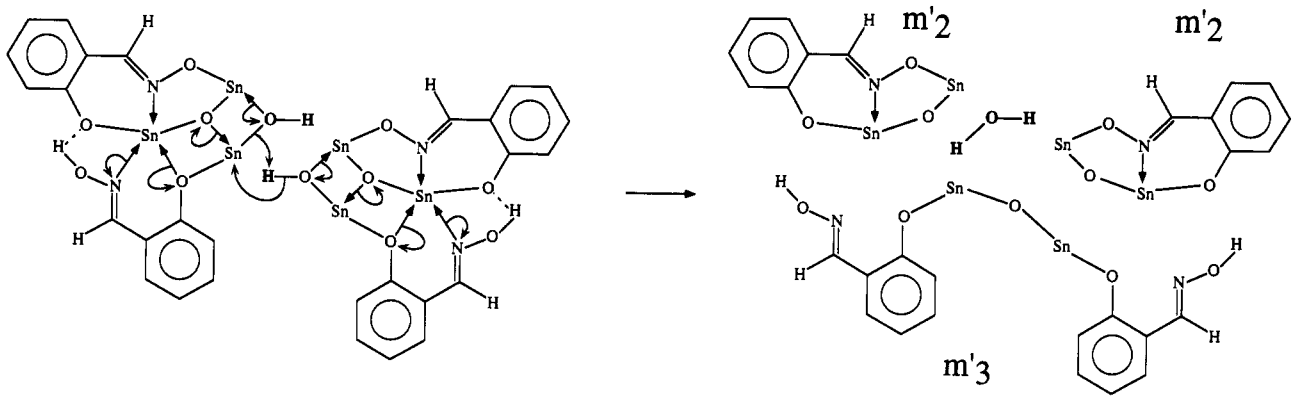

Figure 14. Possible mechanism for the formation of species m'_2 and m'_3 from the major species M. The butyl groups have been omitted for clarity.

Solution Chemistry. The generation of the species m_1, m_2, and m_3 through eqs 1–4 would require the involvement of free salicylaldoxime and di-*n*-butyltin oxide moieties. Such an involvement is not supported by our experimental data, which show m_1, m_2, and m_3 to be generated spontaneously from M upon dissolution of pure crystals of 1, without any noteworthy amounts of Bu_2SnO and HONZOH in the equilibrium mixture. Only over the long term do traces of a precipitate (believed to be Bu_2SnO) sometimes appear in the solution of 1, which is easily dissolved upon heating, showing the reversible nature of this undesired side reaction. Upon enhanced generation of m_1 and m_2 at higher temperatures, on the other hand, we did observe small droplets of water appearing in the C_6D_6 solution of the sealed NMR tube. Furthermore, Figure 8b shows that addition of dry zeolites removes the water from the equilibrium mixture and shifts the equilibrium toward the species m_1 and m_2. Figure 14 proposes one possible mechanism that accounts for the "spontaneous" decomposition of M. The mechanism starts with elimination of water from the O40–H groups of two molecules of M. This gives rise to a new distannoxane bridge in the intermediate m'_3, with elimination of 2 equiv of an intermediate m'_2, according to the equation

$$2M \rightleftharpoons m'_3 + 2m'_2 + H_2O \qquad (5)$$

The dimerization, according to eq 4, of m'_3, which has the formula $[(Bu_2Sn)(Bu_2SnO)(HONZO)_2]$, explains the generation at room temperature of a small amount of m_3 in solution.

On the other hand, the intermediate m'_2, $[(Bu_2Sn)(Bu_2SnO)(ONZO)]$, released likewise from reaction 5, is the monomer of m_2. Henceforth, as for m'_3, the generation of m_2 is easily explained by simple dimerization of m'_2 as well.

Another fate for the intermediate m'_3 allows us now to explain the generation of m_1. Thus, the chemical reaction according to which this can occur

$$M + m'_3 \rightleftharpoons m_1 + m'_2 + H_2O \qquad (6)$$

is easily understood if it is rewritten as

$$\underset{M}{[(Bu_2Sn)(Bu_2SnO)(\boldsymbol{Bu_2SnOH})(HONZO)(ONZO)]} + \underset{m'_3}{[(Bu_2Sn)(Bu_2SnO)(\boldsymbol{HONZO})_2]} \rightleftharpoons \underset{m_1}{[(Bu_2Sn)_2(Bu_2SnO)(HONZO)_2(ONZO)]} + \underset{m'_2}{[(Bu_2Sn)(Bu_2SnO)(\boldsymbol{ONZO})]} + \boldsymbol{H_2O}$$

The latter view on reaction 6 corresponds globally to a simple transfer of a HONZO moiety from m'_3 to M, coupled with the elimination of one molecule of H_2O. Thus, m'_3 and m'_2 differ formally by one HONZO unit, one H^+ equivalent having been lost during the conversion from m'_3 to m'_2. Accordingly, M and m_1 differ by the OH group of the Bu_2SnOH moiety of M having been lost, to combine with the above proton to generate the water molecule, and one unit of HONZO having been added during the simultaneous conversion from M to m_1. Figure 15 proposes a simple mechanism in terms of an m'_2 unit being substituted for a m'_3 unit with elimination of water. In this way all the chemical features of M in solution are explained. The increase in temperature just favors the generation of more m_1 and m'_2 (hence m_2), at the expense of M and m'_3 (hence m_3) being further consumed by the reaction 6, as observed experimentally.

Summing eqs 5 and 6 gives rise to

$$3M \rightleftharpoons m_1 + (3/2)m_2 + 2H_2O$$

since m_2 is the dimer of m'_2, and alternatively to

$$6M \rightleftharpoons 2m_1 + 3m_2 + 4H_2O$$

The model just proposed accounts for all the spectroscopic and chemical observations made. Even the reversible formation, over the long term, of traces of Bu_2SnO, as observed in the NMR samples, can be straightforwardly accounted for by the side reaction

$$M + m'_2 \rightleftharpoons m_1 + (2/n)(Bu_2SnO)_n$$

Many other intermediate combinations can be conceived to generate the observed species, but in order to avoid lengthy mechanistic discussions, we confine ourselves to the conceptually least complex one proposed here.

Conclusion

There is no doubt that the major species M in solution has the same structure as compound 1 in the solid state even if it can be the subject of tautomeric proton transfers. The minor solution transients m_1, m_2, and m_3 could not be isolated as pure compounds and, henceforth, be better characterized. Their structures are, however, the subject of only slight uncertainty. Thus, the fascinating solution chemistry of compound 1 appears to be explainable in a self-consistent network of reactions involving the four main species observed (M, m_1, m_2, and m_3) and giving rise only to associations, dissociations, and/or transfers of protons and salicylaldoximate moieties, as well as to generation of

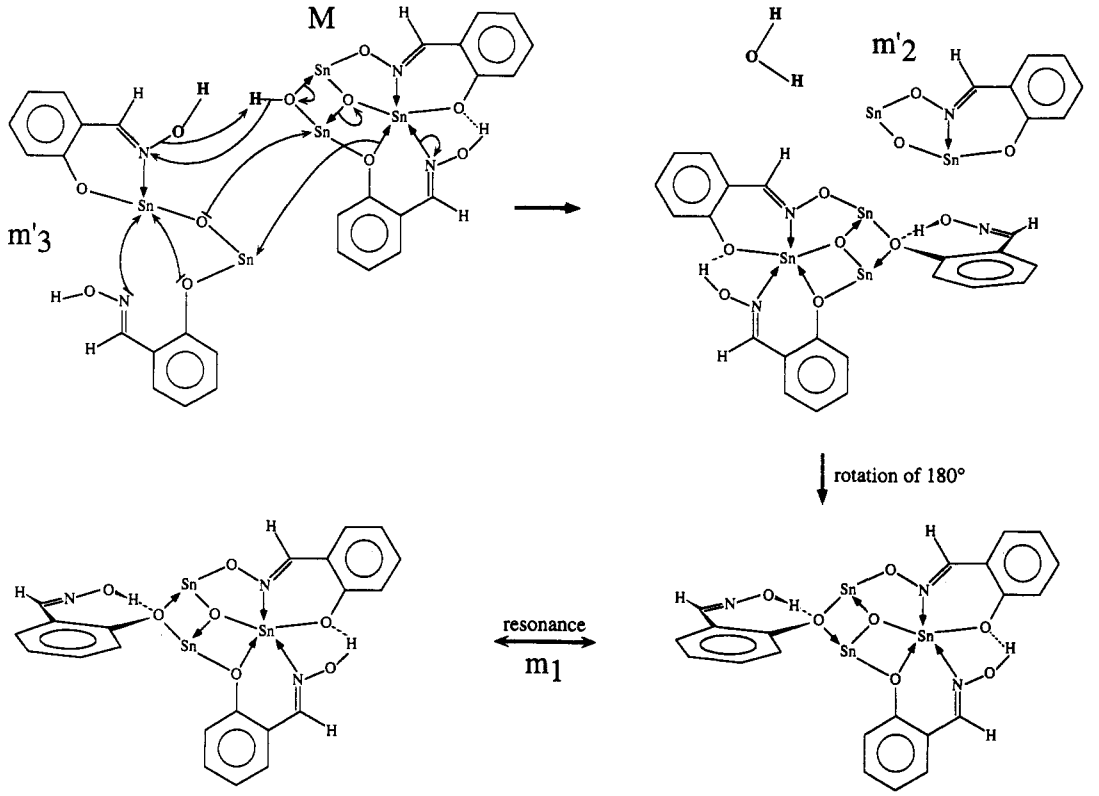

Figure 15. Possible mechanism for the formation of m_1 from M by substitution of an m'_2 unit for an m'_3 unit. The butyl groups have been omitted for clarity.

water. Moreover, all these structures receive major support from accurate NMR data obtained by proton detected 2D ^1H–^{119}Sn HMBC spectroscopy. Obviously, the latter technique,[6] applied to the tin-119 nucleus,[7] opens powerful perspectives in the structure elucidation of organotin compounds in solution. The main tool in this determination is the observation of very long range couplings involving tin-119 and hydrogen-1 nuclei.

Experimental Section

Synthesis. In a typical synthesis experiment, di-*n*-butyltin oxide (0.03 mol) and salicylaldoxime (0.02 mol) were refluxed in a mixture of 100 mL of ethanol and 400 mL of toluene. The ternary azeotrope water/ethanol/toluene was distilled off with a Dean–Stark funnel. After 6 h, the solvent was evaporated. The solid obtained was recrystallized from *n*-hexane, cyclohexane, or acetonitrile (yield 91%; mp 92–94 °C). Anal. Found: C, 45.8; H, 6.95; N, 2.57. Calcd for $C_{38}H_{66}O_6N_2Sn_3$: C, 45.5; H, 6.63; N, 2.79.

X-ray Diffraction Analysis. Details are given in Table 7.

NMR experiments. The samples were prepared under air- and moisture-free conditions in NMR tubes, which were afterwards sealed, by dissolving typically *ca.* 100 mg of **1** in 0.5 mL of C_6D_6. All the 1D spectra were recorded using standard program and parameter sets available in the Bruker microprogram library on a Bruker AC250 instrument operating at 250.13-MHz proton frequency and equipped with a QNP (^1H, ^{19}F, ^{13}C, ^{119}Sn) probe and on a Bruker AMX500 spectrometer operating at 500.13-MHz proton frequency.

Totally deuterated samples were prepared by dissolving **1** in CD_3OD and subsequently evaporating the methanol under reduced pressure. The HO:DO ratio for the ^1H and ^{119}Sn SIMPLE-NMR experiments was adjusted to 60:40 by adding 40 mg of the totally deuterated sample to a 0.5-mL C_6D_6 solution of the totally protonated sample (60 mg).

The ^{13}C–^1H HETEROCOSY and the ^1H–^{13}C HMQC-RELAY spectra were obtained on the AMX500 instrument equipped with an inverse-detection triple-resonance (^1H, ^{13}C, ^{15}N) probe head and using the standard pulse sequences from the Bruker microprogram library.

Table 7. Experimental X-ray Diffraction Data with Structure Refinement Parameters

Crystallographic Data	
formula unit	$C_{38}H_{66}O_6N_2Sn_3$
syst	monoclinic
space group	$P2_1/c$
unit cell	
a (Å)	20.995(3)
b (Å)	17.394(4)
c (Å)	12.254(2)
β (deg)	94.43(2)
V (Å^3)	4462(1)
Z	4
D_{calcd} (g cm^{-3})	1.49
μ(Cu Kα) (cm^{-1})	131.97
(b) Data Collection (295 K)	
cryst size (mm)	0.25 × 0.2 × 0.1
four-circle diffractometer	Huber
radiation	Cu Kα
λ (Å)	1.5418
monochromator	graphite
scan mode (width (deg))	θ–2θ (1.8)
2θ range (deg)	3–135
hkl range: min; max	–25, 0, 0; 24, 20, 13
no. of indep rflns	
measd	8043
obsd ($I > 2.5\sigma$)	3135
empirical abs cor (ψ scan)	
min abs cor	0.542
max abs cor	0.906
(c) Structure Determination and Refinement[a]	
method used to solve structure	direct methods (SHELX86)[18]
refinement	anisotropic least squares using F (SHELX76)[19]
weighting scheme	$w = [\sigma^2(F) + 0.00110F^2]^{-1}$
R, R_w, S	0.062, 0.061, 1.158
max, min height in final DF map (e Å^{-3})	0.71, –0.70
max Δ/σ in the last cycle	0.07

[a] No H atoms were located.

The 2D proton detected ^1H–^{13}C HMQC-RELAY spectrum was recorded using the pulse sequence and phase cycling proposed by Lerner and Bax[11] using ^{13}C decoupling (GARP[17]). Decoupling was started at the same time as the acquisition after the final 90° proton pulse. This maintains the correlations via one-bond couplings, but they were attenuated by choosing an initial evolution delay of 5 ms. The experiment was optimized to a $^1J(^1H–^{13}C)$ value of 143 Hz. A total of 411 FID's were recorded and zero-filled to 2 K in the F_1 dimension with a spectral width of 5660 Hz centered at the middle of the ^{13}C spectrum. The resulting folding in F_1 was necessary to achieve the needed resolution. Because in this special case the different coupling networks are independent and are not overlapping in F_1 or in F_2, folding did not complicate the interpretation of the spectrum. In the F_2 dimension, 4K data points, no zero-filling, a spectral width of 4504 Hz (0.0–9.0 ppm; acquisition time 455 ms), 64 scans, and a relaxation delay of 1 s were used.

The 2D proton detected ^1H–^{119}Sn HMBC-COSY spectra were recorded on the Bruker AC250 spectrometer using the QNP probe head and were processed on the AMX500 instrument. Two variants were run on the sample equilibrated at room temperature: with and without ^{119}Sn decoupling using the pulse sequences and phase cycling proposed by Bax and Summers.[6] An additional spectrum without ^{119}Sn decoupling was recorded after preheating the sample for 48 h and cooling it to room temperature prior to acquisition. The experiments were optimized to $^nJ(^1H–^{119}Sn)$ average values of 8 Hz (delay 62 ms). No low-pass J filter was used. A total of 256 FID's were recorded and zero-filled to 2K in the F_1 dimension with a spectral width of 18 648 Hz (–300 to –500 ppm). The resulting folding (see Results) in F_1 was necessary to achieve the needed resolution. In the F_2 dimension, 4K data points, no zero-filling, a spectral width of 4098 Hz (acquisition time 500 ms), 128 scans, and a relaxation delay of 1.5 s were used.

Mössbauer Spectroscopy. The Mössbauer spectrum was recorded with the constant-acceleration mode and with a $Ca^{119m}SnO_3$ source from Amersham, using a homemade (INAN, Université Catholique de Louvain) instrument designed and built by the "Instituut voor Kern- en Stralingsfysika" (IKS), Leuven, Belgium. The probe was maintained at a temperature between 90 and 100 K and the source at room temperature. The digital data were treated with a least-squares iterative program, deconvoluting the spectrum as a combination of Lorentzians.

Acknowledgment. We thank Prof. B. Mahieu (Catholic University of Louvain, Louvain-la-Neuve, Belgium) for recording the Mössbauer spectrum, Prof. G. Natile (University of Bari, Bari, Italy) for performing the elemental analysis, and Mr. W. Verbist, Mr. A. Verwee, and Mrs. I. Verbruggen (Free University of Brussels, VUB) and Dr. R. Ottinger (Free University of Brussels, ULB) for recording NMR spectra. A useful discussion with Dr. J. G. Wolf of the "Université Paul Sabatier", Toulouse, France, is gratefully acknowledged. Financial support from the Belgian "Nationaal Fonds voor Wetenschappelijk Onderzoek" (Grant FKFO 20127.90; M.G. and R.W.), from the Belgian "Nationale Loterij" (Grant 9.0050.90; R.W. and M. Biesemans), from the Moroccan "Ministère de l'Education Nationale du Maroc" (M. Bouâlam and A.E.), from the "Ministère des Affaires Culturelles du Luxembourg" (Grant number BFR90/036) (F.K.), from the "Comité National des Bourses OTAN" (F.K.), and from the "Ministère de l'Education Nationale du Luxembourg" (F.K.) is gratefully acknowledged. Valuable suggestions of the reviewers are gratefully acknowledged.

Supplementary Material Available: An ORTEP plot giving the full numbering scheme, including the *n*-butyl groups, and tables of anisotropic thermal parameters and all bond distances and angles for **1** (5 pages). Ordering information is given on any current masthead page.

OM930480L

(17) (a) Shaka, A. J.; Barker, P. B.; Freeman, R. *J. Magn. Reson.* **1985**, *64*, 547. (b) Barker, P. B.; Shaka, A. J.; Freeman, R. *J. Magn. Reson.* **1985**, *65*, 535.

(18) Sheldrick, G. M. In *Crystallographic Computing 3*; Sheldrick, G. M., Kruger, C., Goddard, R., Eds.; Oxford University Press: Oxford, U.K., 1985; pp 175-189.

(19) Sheldrick, G. M. SHELX76 Program for Crystal Structure Determination; University of Cambridge: Cambridge, U.K., 1976.